Spatial population structure determines extinction risk in climate-induced range shifts

Manuscript elements: Figures 1-6, online appendices A and B (including figures A1-A3, tables A1-A4, and figures B1-B10). All figures should print in color.

Keywords: range shifts, extinction, rapid evolution, dispersal evolution, individual-based model

Manuscript type: Article.

Prepared using the suggested LaTeX template for *Am. Nat.*

Abstract

Climate change is an escalating threat facing populations around the globe, necessitating a robust understanding of the ecological and evolutionary mechanisms dictating population responses. However, populations do not respond to climate change in isolation, but rather in the context of their existing ranges. In particular, spatial population structure within a range (e.g. trait clines, starkness of range edges, etc.) likely interacts with other ecological and evolutionary processes during climate-induced range shifts. Here, we use an individual-based model to explore the interacting roles of these factors in range shift dynamics. We show that increased spatial population structure (driven primarily by a steeper slope in an environmental gradient) severely increased a population's extinction risk. Further, we show that while evolution of heightened dispersal during range shifts can aid populations in tracking changing conditions, it can also interact negatively with adaptation to the environmental gradient, leading to reduced fitness and contributing to the increased extinction risk observed in populations structured along steep environmental gradients. Our results demonstrate that the effect of dispersal evolution on range shifting populations is dependent on environmental context and that spatial population structure can substantially increase extinction risk in range shifts.

Introduction

Climate change is expected to dramatically reshape global biogeographic patterns as some species shift their ranges to track changing environmental conditions (Gonzalez et al., 2010). These range shifts are generally predicted to proceed upwards in latitude, elevation, or both as average global temperatures continue to rise (Loarie et al., 2009). Indeed, contemporary range shifts have already been observed in a wide variety of taxa, from algae to mammals (Chen et al., 2011; Parmesan, 2006). Such range shifts present significant challenges to current and future conservation efforts as they can result in the extinction of populations failing to track a changing climate (Parmesan, 2006) as well as the creation of novel species assemblages (Hobbs et al., 2009). Understanding the ecological and evolutionary dynamics of such climate-induced range shifts will play a key role in informing current and future conservation work.

Large-scale population movements have been studied for decades in the broader context of range expansions, leading to a robust understanding of both the ecological (Hastings et al., 2005) and evolutionary (Excoffier et al., 2009; Shine et al., 2011) mechanisms shaping such expansions. For example, while range expansion speed can be well approximated by a combination of the species' intrinsic growth rate and dispersal ability (Fisher, 1937; Hastings et al., 2005), recent research demonstrates that evolution in these traits can increase both the mean and variance of expansion speed through time (Phillips, 2015; Shaw and Kokko, 2015; Szűcs et al., 2017). In particular, laboratory experiments have shown spatial genetic structure to play an important role in the dynamics of range expansions, even over short time periods (Ochocki and Miller, 2017; Weiss-Lehman et al., 2017). While some range expansions (e.g. of invasive or reintroduced species) start from small founding populations lacking any initial spatial structure, others are characterized by far more complex initial spatial population structure (e.g. humans expanding out of Africa

or expansions following glacial retreat). Climate-driven range shifts fall in the latter category, as populations respond to climate change in the context of preexisting spatial population structure. For example, species' ranges may be characterized by spatial clines in abundance and genetic patterns. Such clines can form in response to a number of extrinsic or intrinsic factors including adaptation to environmental gradients (Kirkpatrick and Barton, 1997), altered demographic rates throughout the range (Holt et al., 2005), or interactions with other species (Case and Taper, 2000). Importantly for climate-driven range shifts, the factors influencing these spatial patterns will likely shift with the changing climate, causing simultaneous range contraction and expansion at opposite range margins. Thus, climate-driven range shifts will be affected both by the eco-evolutionary dynamics known to impact range expansions and the moving constraints on spatial population structure impacted by changing climatic conditions.

Certain aspects of spatial population structure have the potential to affect the dynamics of range shifts under changing climatic conditions. For example, the underlying mechanism causing population declines at the range edge (e.g. declines in carrying capacity versus growth rate) can alter a population's extinction risk during climate driven range shifts (Henry et al., 2013). Further, in ranges characterized by a gradient in a trait optimum, the starkness of the range edge can impact the ability of peripheral populations to adapt to the local optimum, with stark range edges leading to better adaptation in peripheral populations (García-Ramos and Kirkpatrick, 1997), though the importance of this for range shifts has not been investigated. Additionally, the nature of dispersal can interact with adaptation to a trait optimum gradient to impact range shift dynamics. When dispersal occurs in a stepping stone manner, maladapted individuals (i.e. individuals whose phenotypes do not match the local optimum) can block the establishment of better adapted genotypes so long as the mismatch is not too severe (Atkins and Travis, 2010). While these aspects of spatial population structure have been shown to impact the dynamics of climate-induced range shifts in

isolation, it is unclear how and if they might interact.

Further, given the importance of rapid trait evolution in range expansions (Ochocki and Miller, 2017; Phillips, 2015; Shaw and Kokko, 2015; Szűcs et al., 2017; Weiss-Lehman et al., 2017), it is necessary to consider the interplay between aspects of spatial population structure and the role of rapid evolution during range shifts. In asexual species, for example, local adaptation to an environmental gradient has been shown to interact with dispersal evolution during climate change, driving increased dispersal probability as genotypes shift to keep pace with their environmental optimum (Hargreaves et al., 2015). However, it is unclear how these two processes might interact in a sexually reproducing species in which dispersal and local adaptation are directly linked via gene flow. Under sexual reproduction, evolution of increased dispersal could simultaneously reduce adaptation to an environmental gradient due to increased gene flow throughout the range (García-Ramos and Kirkpatrick, 1997; Kirkpatrick and Barton, 1997). In fact, long-distance pollen dispersal in flowering plants is predicted to restrict local adaptation and, when pollen dispersal sufficiently outpaces seed dispersal, to lead to ecological niche shifts rather than spatial range shifts in response to climate change (Aguilée et al., 2016). In addition to potential interactions between adaptation and dispersal evolution, the starkness of the range edge could influence the potential for rapid trait evolution during range shifts by altering the spatial distribution of dispersal phenotypes throughout the range (Hargreaves and Eckert, 2014; Henry et al., 2013), thus altering the diversity of dispersal genotypes present for subsequent evolution during range shifts.

Here, we assess the interaction of two mechanisms responsible for spatial population structure (edge type and an environmental gradient in a trait optimum) with trait evolution in sexually reproducing populations undergoing range shifts. We developed an individual-based model capable of producing a wide variety of spatial population structures in which males and females were defined by two genetically determined traits, thus allowing for both evolutionary and ecological responses

to climate change. One trait determined dispersal ability while the second allowed for adaptation to the environmental gradient. Using this model, we varied both the environmental gradient in the trait optimum and the starkness of the range edge to ascertain how they interact with each other and with the process of trait evolution to impact a population's ability to track a changing climate. Previous research suggests evolution of heightened dispersal during the range shift might alleviate the extinction risk of moving populations (Boeye et al., 2013; Hargreaves et al., 2015; Henry et al., 2013), but we predicted steep environmental gradients and stark range edges may inhibit such evolution and thus increase extinction risk.

Methods

A full description of the individual-based model using the Overview, Design concepts, and Details protocol (Grimm et al., 2010) is available in Appendix A, while we present a brief summary here. Population dynamics occurred within discrete habitat patches embedded in a two dimensional lattice in which environmental conditions varied along the x dimension but remained constant along the y dimension (Fig. A1). Landscapes were unbounded in the x dimension but defined by a fixed width and wrapping boundaries in the y dimension. Abiotic conditions varied along the x dimension of landscapes in two ways. First, a linear environmental gradient determined the optimum phenotype in a quantitative trait, driving adaptation throughout the range. Second, the patch carrying capacities systematically declined from the range center to edge along the x dimension. The starkness of this decline could be altered to create different types of range edges (Fig. A3). While an environmental gradient in a quantitative trait optimum is sufficient to produce stable range limits under certain conditions (Alleaume-Benharira et al., 2006; Kirkpatrick and Barton, 1997; Polechova, 2018; Polechová and Barton, 2015), we included the decline in carrying capacities to enforce stable range limits when the environmental gradient was too shallow to produce

them (Alleaume-Benharira et al., 2006; García-Ramos and Kirkpatrick, 1997). A wide variety of other range limiting mechanisms have been proposed, including interspecific interactions (Case and Taper, 2000; Price and Kirkpatrick, 2009), Allee effects (Keitt et al., 2001), and spatial variation in demographic parameters (Holt et al., 2005) among others. Given empirical evidence for many different range limiting mechanisms (Gaston, 2009), the inclusion of both an environmental gradient in the trait optimum and the decline in carrying capacities allowed the model to capture a wide variety of spatial population structures, including ranges not structured by adaptation to an environmental gradient, with minimal additional assumptions. Previous research has shown that using a decline in intrinsic growth rate as opposed to carrying capacity may impact extinction risk but does not alter the patterns of dispersal evolution during climate change (Henry et al., 2013). To maintain generality, we do not assume a specific mechanism behind the decline in carrying capacity, but it could represent a variety of range limiting mechanisms such as physiological limits to adaptation, the effects of competition, or underlying resource distributions (Case and Taper, 2000; Holt et al., 2005; Price and Kirkpatrick, 2009; Sexton et al., 2009). Thus, the x dimension defined the environmental context of the population and the y dimension allowed for variation in population dynamics under identical environmental conditions. To simulate climate change, the patch carrying capacities and the environmental gradient shifted at a constant rate along the x dimension. Generations were non-overlapping and consisted of discrete dispersal and reproduction phases (Fig. A2).

Individuals were characterized by two traits, each defined by a set of 5 quantitative diploid loci. While the number of loci was arbitrary, 5 was chosen as a compromise between computational restrictions and the likely polygenic nature of such complex traits. The first trait defined an individual's expected dispersal distance, assuming an exponential dispersal kernel. An individual's realized dispersal distance was then drawn from the dispersal kernel and dispersal direction was

135 random and unbiased. Dispersal occurred in continuous space from the center of an individual's current patch and the individual's new patch was then determined by the mapping from continuous space to discrete patches (see Appendix A). The second trait allowed for adaptation to the 138 local conditions along the environmental gradient. The environmental gradient determined the local phenotypic optimum in this trait and deviation from this optimum decreased individual fitness. As this trait determined the environmental conditions in which individuals would experience max- 141 imal fitness, we refer to it as the niche trait when differentiating between it and the dispersal trait. Reproduction within each patch occurred via a stochastic implementation of the classic Ricker model (Melbourne and Hastings, 2008; Ricker, 1954), scaled by the mean fitness of the patch. 144 Parental pairs formed via random sampling of the local population (with replacement) weighted by individual fitness such that individuals with a close match of their niche trait to the local optimum produced more offspring on average. Thus, the model used a mixture of hard selection (realized 147 population growth declined with maladaptation to the environmental gradient) and soft selection (probability of producing offspring depended on fitness relative to other individuals) for the evolutionary dynamics (Wallace, 1975). Allele inheritance was subject to mutation and assumed no 150 linkages among loci. The mutation process was designed such that mutational input per generation was independent of the number of loci (see Appendix A) and with parameters corresponding to previous estimates from the literature (Gilbert et al., 2017).

153 We varied parameter values to explore the interacting roles of the slope of the environmental gradient and different types of range edges (Table A2) in forming spatial population structure at equilibrium and driving the subsequent eco-evolutionary dynamics of range shifts. Specifically, 156 we considered a fully factorial combination of: (1) a flat, shallow, and steep environmental gradient, (2) gradual, moderate, and stark declines in carrying capacity at the range edge, and (3) slow, moderate, and fast speeds of climate change. This yielded a total of 27 different scenarios, each

explored with 200 simulations, during which we tracked the mean phenotypes of both traits and their genetic variances in each patch through time. The first 2000 generations of each simulation allowed populations to reach a spatial equilibrium, which we confirmed by assessing the spatial distributions of phenotypes and genetic variances in both traits for stability through time. On average, simulations in every scenario arrived at stable distributions in all values by generation 1500. Following the initial 2000 generations, we imposed 100 generations of climate change by shifting the environmental gradient and patch carrying capacities at a constant rate. Figure 1 shows an example of a single population responding to a moderate speed of climate change. For each scenario, we evaluated the impact of the environmental gradient and edge type on trait evolution and extinction dynamics during the range shift. We primarily discuss simulations assuming a moderate speed of climate change in the main text, but present the results for slow and fast speeds of climate change in Appendix B. To assess spatial patterns in trait evolution, we focused primarily on variation along the x dimension of simulated landscapes for two reasons: (1) to capture variation relevant to the changing environmental conditions and (2) because variation in this dimension was much greater than variation within the y dimension in all scenarios. All simulations and data processing were performed in R version 3.4.4 (Team, 2000) and the code is available at (links are available from the journal office).

Results

Extinction

Extinction dynamics during the climate-driven range shifts varied widely among scenarios, ranging from no extinctions in some scenarios to the extinction of every simulated population in others. We quantified extinction probability in each scenario as the proportion of simulated populations

to decline to extinction through time during the 100 generations of climate change. Comparing extinction probabilities among scenarios revealed four prominent patterns. First, the slope of the environmental gradient strongly impacted extinction risk (Fig. 2). Scenarios with a flat gradient only resulted in extinctions at a fast speed of climate change coupled with a stark range edge (Fig. B2), while scenarios with a steep gradient experienced high extinction probabilities at even a slow speed of climate change (Fig. B1). Second, edge type also had an important effect on extinction probability, with stark edges increasing extinction risk over gradual and moderate edges. Interestingly, when scenarios with moderate and gradual range edges diverged in extinction probabilities, moderate edges consistently yielded lower extinction risk than scenarios with gradual edges (Fig. 2, B1, & B2). Third, while both the environmental gradient and edge type influenced extinction probabilities, the environmental gradient drove more dramatic changes to extinction risk. We varied both parameters widely among scenarios, doubling the slope of the environmental gradient and increasing edge starkness by a factor of 100 (Table A2). Thus, our results suggest the environmental gradient is the stronger driver of extinction risk during climate-induced range shifts across a wide region of parameter space and corresponding biological scenarios. Finally, as expected, the speed of climate change also influenced extinction probability with faster climate change corresponding to greater extinction risk (Fig. B1 & B2).

Dispersal evolution

The distribution of dispersal phenotypes at spatial equilibrium varied across the x dimension of simulated landscapes, with more dispersive phenotypes characterizing the range edges. While this pattern held generally across all scenarios, the difference between edge and core phenotypes was reduced in the presence of an environmental gradient and starker range edges, leading to lower dispersal phenotypes at the range margins in these populations (Fig. 3). At equilibrium, the dis-

tributions of dispersal phenotypes were symmetric, but spatial sorting not only increased dispersal phenotypes in surviving populations, but led to asymmetric distributions with the highest phenotypes at the leading edge. Despite these initial changes, the spatial distributions remained remarkably stable between 50 and 100 generations, regardless of the speed of climate change (Fig. 3, B3, & B4). This stands in contrast to models of dispersal evolution in unbounded range expansions, which predict dispersal to continually increase as the expansion progresses (Fronhofer and Altermatt, 2015; Shaw and Kokko, 2015; Shine et al., 2011). In our model, the shifting environmental gradient and distribution of carrying capacities simultaneously exposed new habitat for colonization, thus allowing spatial sorting, and also reduced the fitness of individuals that dispersed too far, resulting in an upper limit on dispersal evolution.

Both the severity of the environmental gradient and edge starkness also determined the spatial distribution of genetic variance in the dispersal trait. Increasing the slope of the environmental gradient reduced the genetic variance in dispersal across the range, but did not alter the qualitative patterns. The type of range edge, on the other hand, qualitatively altered the spatial distribution of genetic variance in dispersal (Fig. 4). Scenarios with gradual and moderate edges displayed similar patterns of heightened variance at the range center compared to the margins, but stark edges resulted in the opposite pattern. This discrepancy makes sense as scenarios with stark declines in carrying capacity lacked the low abundance, and hence low genetic variance, populations that characterized the edges of scenarios with gradual or moderate declines in carrying capacity (Fig. A3). In all scenarios, genetic variance in dispersal decreased throughout the range in response to climate change (Fig. 4), consistent with selection for increased dispersal via spatial sorting. This pattern was qualitatively similar for all speeds of climate change (Fig. B5 & B6).

Adaptation to the environmental gradient

Equilibrium values of the niche trait closely matched the environmental gradient in the range core and diverged at the edges (Fig. 5), likely due to a combination of gene swamping from abundant central populations (Kirkpatrick and Barton, 1997) and the loss of genetic diversity due to drift in small, peripheral populations (Polechova, 2018; Polechová and Barton, 2015). In agreement with previous results, the starkness of the range edge influenced this pattern, with increased maladaptation of peripheral populations in scenarios with gradual edges (García-Ramos and Kirkpatrick, 1997). Across all scenarios, the clines in the niche trait became substantially shallower during the range shift (Fig. 5). As a result, the match between the environmental gradient and local trait values substantially deteriorated during climate change, resulting in reduced fitness across most of the range. This reduction in fitness, observed at all speeds of climate change (Fig. B7 & B8), could partially explain the increased extinction probability observed for scenarios with a steep environmental gradient (Fig. 2).

In contrast to the dispersal trait, genetic variance in the niche trait at equilibrium actually increased with the slope of the environmental gradient (Fig. 6). This is likely due to the increased range of environmental conditions encountered by populations arranged along a steeper environmental gradient. The spatial distributions of genetic variance in the niche trait were qualitatively similar for scenarios with moderate and stark edges, peaking at the center of the range and declining towards the edges. However, scenarios with gradual edges displayed different patterns in the genetic variance of the niche trait, with a peak in variance occurring between the range center and each edge (Fig. 6). This pattern was lost during range shifts, though, leading to qualitatively similar distributions of genetic variance in the niche traits among different edge types (Fig. 6). In contrast to the loss of genetic variance observed in the dispersal trait during climate change, the magnitude

of genetic variance in the niche trait during climate change was roughly equivalent to that characterizing equilibrium populations in most scenarios, regardless of the speed of climate change (Fig. B9 & B10). Only in scenarios with gradual edges did genetic variance decrease slightly in response to climate change

Discussion

Range shifts due to climate change represent a global threat to biodiversity and much recent research has focused on exploring the underlying ecological and evolutionary dynamics of such range shifts to inform conservation efforts. Here we showed that extinctions due to climate-induced range shifts are more likely in populations structured by steeper environmental gradients or starker range edges. For our approach, we developed an individual-based model to explore the eco-evolutionary dynamics of climate-induced range shifts in sexually reproducing, diploid populations with both dispersal and niche traits defined by multiple loci. In contrast, previous models have focused on a subset of these factors: ecological dynamics (e.g. (Brooker et al., 2007)), evolution in a single trait only (e.g. (Atkins and Travis, 2010; Henry et al., 2013)), and relatively simple genetic scenarios (e.g. single-locus haploid genetics in asexual populations (Boeye et al., 2013; Hargreaves et al., 2015)). Previous studies on eco-evolutionary dynamics of populations responding to climate change have generally predicted that evolution of increased dispersal might provide relief for populations struggling to keep pace with changing environmental conditions (Boeye et al., 2013; Hargreaves et al., 2015; Henry et al., 2013). Here, we tested the generality of these predictions in populations with varying types of spatial structure induced by the underlying environmental conditions.

While all surviving populations evolved increased dispersal phenotypes during range shifts, the environmental gradient and edge starkness may have hampered the ability of populations to

achieve such increases in dispersal under certain scenarios. For example, scenarios characterized by
273 stark edges or steep environmental gradients led to edge populations composed of lower dispersal phenotypes at equilibrium due to the increased cost of dispersal in these scenarios. In the presence of a steep environmental gradient, selection favors lower dispersal phenotypes due to the fitness
276 cost of dispersing to a location with a drastically different environmental optimum (Kirkpatrick and Barton, 1997). Similarly, stark range edges can select for lower dispersal due to the increased risk of dispersing into unfavorable habitat (Shaw et al., 2019, 2014). Previous research has documented
279 a similar reduction in dispersal phenotypes due to an explicit mortality cost of dispersal (Kubisch et al., 2013), whereas the costs to dispersal in our model result from the environmental gradient and range edge starkness. By starting from lower dispersal phenotypes, populations structured by steep
282 environmental gradients or stark range edges needed to achieve greater evolutionary increases in dispersal, since populations in all scenarios evolved to similar levels of dispersal in response to climate change (Fig. 3). Presumably, the increased magnitude of the required evolutionary change
285 in dispersal might have contributed to the increased extinction risk observed in such scenarios.

Additionally, both the environmental gradient and the edge starkness impacted the spatial distribution of genetic variance in dispersal at equilibrium, thus altering the evolutionary potential
288 of populations in different scenarios. Equilibrium genetic variance in dispersal decreased with an increasingly steep environmental gradient. Coupled with the reduced dispersal phenotypes characteristic of these scenarios at equilibrium, this reduction in genetic diversity could have amplified the
291 difficulty of populations evolving the increased dispersal necessary to track climate change. While the effect of edge type on equilibrium patterns of genetic variance in dispersal was less straightforward, resulting in qualitative differences among different levels of edge starkness, it provides a clue
294 to the lower extinction risk faced by scenarios defined by moderate versus gradual edges (Fig. 2). Scenarios defined by moderate edges consistently had higher levels of genetic variance in dispersal

compared to scenarios with gradual edges, suggesting the evolution of increased dispersal during range shifts may have been easier in such scenarios.

Adaptation to the environmental gradient and patterns in the genetic variance of the niche trait in the different scenarios likely contributed to the extinction risk of range shifting populations as well. The process of shifting in response to climate change resulted in dramatically increased mismatches between the environmental gradient and local phenotypes (Fig. 5), thus reducing fitness throughout the range. While this pattern resulted from the shifting locations of the environmental optima, it was likely exacerbated by heightened gene flow throughout the range driven by the increased dispersal phenotypes evolved during range shifts (Lenormand, 2002). This means even the populations successfully tracking climate change experienced substantially reduced fitness relative to equilibrium, which could partially explain the increased extinction risk characterizing scenarios with steep environmental gradients. Contrary to the dispersal trait, genetic variance in the niche trait did not decline during the range shift, except in scenarios with gradual edges (Fig. 6). This finding agrees with previous theoretical investigations of stable ranges which found that loss of genetic variance due to genetic drift can constrain range expansion in the presence of an environmental gradient (Polechova, 2018; Polechová and Barton, 2015). Thus, a reduction in genetic variance of the niche trait, as observed for scenarios with gradual edges, could constrain a population's ability to track changing environmental conditions. Along with the patterns in genetic variance of the dispersal trait, this could have contributed to the increased extinction risk faced by populations defined by gradual compared to moderate range edges.

Previous models have predicted that dispersal evolution may be capable of rescuing populations that would otherwise be unable to keep pace with climate change (Boeye et al., 2013; Henry et al., 2013). While our results generally agree with this prediction, comparison with results from previous models suggests an important role for the biological context of dispersal evolution in

range shifts. In a model assuming asexual reproduction, adaptation to an environmental gradient increased dispersal evolution during range shifts compared to scenarios with no gradient, contrary to the results presented here (Hargreaves et al., 2015). In sexually reproducing populations, however, the evolution of increased dispersal can have an antagonistic interaction with local adaptation to an environmental gradient. Increased dispersal, and therefore increased gene flow, can reduce adaptation to the gradient via gene swamping (Kirkpatrick and Barton, 1997; Lenormand, 2002). When increased dispersal is necessary to track changing environmental conditions, our results suggest the fitness costs to the population can be severe, contributing to increased extinction risks in the presence of an environmental gradient. Thus, while dispersal evolution may be able to improve a population's ability to track changing conditions, it may also incur a severe cost depending on the environmental context of the population. For the purposes of this investigation, we assumed the environmental gradient shifted spatially with climate change, as would be expected if it corresponded to a gradient in temperature or precipitation (Davis and Shaw, 2001). However, in systems characterized by a gradient defined by other factors (e.g. geography or biotic interactions), the gradient might remain stable or even shift in an opposing direction to climate change. Future research should investigate the impact of an environmental gradient unrelated to climate on extinction risk during range shifts.

Similarly, other factors undoubtedly play important roles in dispersal evolution during range shifts. Different models of range shifting populations have made different assumptions regarding life histories, mutation processes, and the genetic architecture of the dispersal trait, all of which have the potential to significantly alter patterns of dispersal evolution. For example, increasing the rate or effect size of mutation would likely increase the ability of dispersal evolution to improve a population's ability to track climate change. Further, life history has been shown to impact the maintenance of genetic diversity, and hence evolutionary potential, with stage and age-structured

populations shown to harbor greater diversity then populations with non-overlapping generations as modeled here (Ellner, 1996). Populations defined by more complex life histories might, therefore, contain more genetic diversity in dispersal at equilibrium, making evolution of increased dispersal during range shifts more likely. Thus, further research is needed to understand how factors such as genetic architecture, mutational dynamics, and life history might interact to shape the potential for population rescue via dispersal evolution during range shifts.

Previous research has identified multiple factors underlying increased extinction risk during climate change, including niche breadth and range extent (Schwartz et al., 2006; Thuiller et al., 2005). While we did not vary niche breadth in our model, both edge starkness and the severity of the environmental gradient both resulted in decreased range extent and greater extinction probabilities, agreeing with previous findings (Schwartz et al., 2006). Our model framework provides new mechanistic insight, however, indicating that adaptation to an environmental gradient and range edge starkness could be key indicators of increased risk during climate-driven range shifts. A survey of the scientific literature found evidence for local adaption in approximately 71% of studies, suggesting a high prevalence of local adaptation in natural populations (Hereford, 2009). While it is difficult to exactly map adaptation to the environmental gradient to empirical measures of local adaptation, the steepest gradient used in our study resulted in the intrinsic formation of stable range boundaries rather than population collapse, which can occur when the environmental gradient is too steep (Alleaume-Benharira et al., 2006; Kirkpatrick and Barton, 1997; Polechova, 2018; Polechová and Barton, 2015). This suggests the parameters used in the scenarios examined here provide reasonable approximations of empirical patterns. Further, a recent meta-analysis of 1400 bird, mammal, fish, and tree species found no evidence for consistent declines in abundance towards range edges (Dallas et al., 2017), a pattern matching that imposed by the starkest range edges examined here (Fig. A3). While some of these patterns could represent a publication bias,

for example against negative results in studies of local adaptation, they suggest many species may have spatial population structures similar to those imposed by steep environmental gradients or stark range edges in our model. Our model suggests such spatial population structure can dramatically increase extinction risk in the face of climate change, meaning many species may be at greater risk than previously understood.

Conclusion

As climate change continues to threaten populations, communities, and ecosystems (Chen et al., 2011; Gonzalez et al., 2010; Hobbs et al., 2009), it is increasingly important to understand population responses to changing environmental conditions. In particular, a deeper, process-based understanding of extinction risk in range shifting populations will, in turn, allow conservation practitioners to identify those populations most vulnerable to climate-driven range shifts. Our results identify certain range characteristics likely to increase extinction risk during range shifts, such as adaptation to a steep environmental gradient or stark range edges, while providing mechanistic insight into the eco-evolutionary dynamics responsible. Specifically, and in contrast to previous models assuming asexual reproduction, we find an antagonistic relationship between dispersal evolution and adaptation to an environmental gradient. Thus, dispersal evolution in response to climate change can impose significant costs in certain environmental contexts. Future work should continue to examine the circumstances determining the potential for population rescue via dispersal evolution in range shifts. As climate change continues to accelerate (Chen et al., 2017), it is imperative to identify those factors leading to increased extinction risk in range shifting populations, and use that knowledge to develop meaningful conservation strategies to mitigate such risk.

Appendix A: Full model description

Model overview

Purpose

This model tested an evolving population's ability to track a changing climate under a variety of conditions. Specifically, populations were simulated under different combinations of (1) the slope of an environmental gradient and (2) the starkness of the range edge. In all simulations, an individual's dispersal and niche trait were defined by an explicit set of quantitative diploid loci subject to mutation, thus allowing both traits to evolve over time. All simulations began with stable climate conditions for 2000 generations to allow the populations to reach a spatial equilibrium before the onset of climate change. Climate change was then modeled as a constant, directional shift in environmental conditions (see *Submodels* below).

State variables and scales

The model simulated a population of males and females characterized by diploid loci for both their expected dispersal distance and niche trait. Space was modeled as a lattice of discrete patches overlaying a continuous Cartesian coordinate system. Landscapes were two dimensional with a fixed width along the y dimension and without bounds on the x dimension. Environmental conditions varied along the x dimension but remained constant within the y dimension. To avoid edge effects due to the fixed width of the y dimension, the model employed wrapping boundaries such that if an individual dispersed out of the landscape on one side, it would appear at opposite side of the y dimension, but at the same x coordinate. Patches were defined by the location of the patch center in x and y coordinates and a patch width parameter defining the relationship between continuous

Cartesian space and the discrete patches used for population dynamics (*Submodels*).

The model implemented climate change by shifting the location of patch carrying capacities and the environmental gradient along the x dimension of the landscape. Patch carrying capacities were defined by the location of the range center along the x dimension, the starkness of the decline characterizing the range edges, and the width of the range along the x dimension (See Figure A1). The environmental gradient was linear and shifted at the same speed and in the same direction as carrying capacities during climate change.

[Figure A1 goes here]

Process overview and scheduling

Time was modeled in discrete intervals defining single generations of the population (Fig. A2). Within each generation, individuals first dispersed from their natal patches according to their phenotypes. After dispersal, reproduction occurred via a stochastic implementation of the classic Ricker model (Ricker, 1954) taking into account the mean fitness of individuals within the patch. Reproduction occurred via random sampling of the local population (with replacement) weighted by individual relative fitness such that individuals with high relative fitness (as determined by the match between their niche trait and the environmental gradient) were likely to produce multiple offspring while individuals with low relative fitness might not produce any. Individuals inherited one allele from each parent at each loci, assuming independent segregation and a mutation process. After reproduction, all individuals in the current generation perished and the offspring began the next generation with dispersal, resulting in discrete, non-overlapping generations.

[Figure A2 goes here]

Design concepts

Emergence

Emergent phenomena in this model included the spatial distributions of population abundance, trait phenotypes, and the genetic variance in each trait (i.e. the spatial population structure). Additionally, the population dynamics during the range shift, including the extinction process, and the evolutionary trajectories of the dispersal and niche traits were all emergent phenomena in this model.

Stochasticity

All biological processes in this model were stochastic, including realized population growth in each patch, dispersal distances of each individual, and inheritance of loci. Environmental parameters were fixed, however, and the process of climate change (i.e. the movement of patch carrying capacity through time) was deterministic. Thus, the model removed the confounding influence of environmental stochasticity to focus on demographic and evolutionary dynamics of range shifts.

Interactions

Individuals in the model interacted via mating and density-dependent competition within patches. Additionally, the evolutionary trajectories of the two different traits had the potential to interact via the relationship between gene flow (dispersal trait) and local adaptation (niche trait). Further, the niche optimum gradient and range edge starkness could interact with trait evolution both during stable climate conditions and during climate change.

Desired output

After each model run, full details of all surviving individuals at the last time point were recorded (spatial coordinates and loci values for both traits). If a population went extinct during the model run, the time of extinction was recorded. For each occupied patch throughout the simulation, we aggregated data on population size, the dispersal trait, and adaptation to local conditions.

Details

Initialization

The following parameters were set at the beginning of each simulation and formed the initial conditions of the model: the mean and variance for allele values of each trait, initial population size, location of the range center, the number of generations of stationary climate conditions (to reach spatial equilibrium), the number of generations of climate change, and all other necessary parameters for the submodels defined below. Simulated populations were initialized in the center of the range and allowed to spread and equilibrate throughout the range during the period of stable climate conditions. This ensured that the populations reacting to a changing climate truly represented the expected spatial distribution for a given range, rather than the initial parameter values used in the simulation (Table A1). Initial population size was chosen to minimize the risk of stochastic extinction in the early stages of the simulation. The time period required to reach spatial equilibrium was determined by initial simulations examining the spatial distributions of phenotypes and genetic variances of both traits through time. We defined populations as at spatial equilibrium once all of these distributions became stable through time. For all parameter combinations, this point was reached by generation 1500, and thus we chose 2000 generations to provide enough time

for all simulated populations to reach spatial equilibrium prior to imposing climate change. The length of climate change was chosen to allow sufficient time for extinction dynamics to play out in simulated populations. The number of patches defining the y dimension and the relationship between Cartesian space and discrete patches were chosen to allow a reasonable number of patches to contribute to the eco-evolutionary dynamics of range shifts while not proving computationally restrictive.

Submodels

Patch carrying capacities. Patch carrying capacity (K_x) varied along the x dimension of the landscape, attaining its highest value at the range center and declining with distance from the center. Specifically, the carrying capacity at a location x was defined as the product of the maximum potential carrying capacity (K_{max}) and a function $f(x,t)$, where $f(x,t)$ was bounded between 1 and 0 with its highest value corresponding to the range center. $f(x,t)$ was defined as

$$f(x,t) = \begin{cases} \frac{e^{\gamma(x-\beta_t+\tau)}}{1+e^{\gamma(x-\beta_t+\tau)}} & x \leq \beta_t \\ \frac{e^{-\gamma(x-\beta_t-\tau)}}{1+e^{-\gamma(x-\beta_t-\tau)}} & x > \beta_t \end{cases} \tag{A1}$$

where β_t defined the center of the range at time t, τ affected the width of the range, and γ affected the slope of the function at the range edges (See Figure A1). Population dynamics occurred within discrete patches, so to calculate a K_x value for a discrete patch from the continuous function $f(x,t)$, we used another parameter defining the spatial scale of each patch (η). The local carrying capacity of a patch centered on x (K_x) was then calculated as the mean of $f(x,t)$ over the interval of the patch multiplied by K_{max}.

$$K_x = \frac{K_{max}}{\eta} \int_{x-\frac{\eta}{2}}^{x+\frac{\eta}{2}} f(x,t)dx \tag{A2}$$

To understand the relationship between γ and the slope of $f(x,t)$ at the range edge, we calcu-

Parameter	Description	Value
N_1	Initial population size (seeded across multiple patches) when beginning the simulations	2500 individuals
β_1	Center of the range during stable climate conditions	0
$\hat{t}$	Duration of stable climate conditions	2000 generations
t_Δ	Duration of climate change	100 generations
t_{max}	Total number of generations in the simulation	2150 generations
η	Width of square habitat patches in Cartesian space	50
y_{max}	Number of patches the discrete lattice extends in the y dimension	10 patches

Table A1: Values and descriptions for parameters determining the initial conditions of simulations, the timing of climate change, and the relationship between Cartesian space and the lattice of discrete habitat patches.

lated the partial derivative of $f(x,t)$ over the x dimension as

$$\frac{\partial f(x,t)}{\partial x} = \begin{cases} \frac{\gamma e^{\gamma(x-\beta_t+\tau)}}{(1+e^{\gamma(x-\beta_t+\tau)})^2} & x \leq \beta_t \\ \frac{-\gamma e^{-\gamma(x-\beta_t-\tau)}}{(1+e^{-\gamma(x-\beta_t-\tau)})^2} & x > \beta_t \end{cases} \tag{A3}$$

yielding a value of $\pm\frac{\gamma}{4}$ at the inflection points on either side of the range center ($x = \beta_t \pm \tau$). Thus, altering γ directly altered the range edge starkness. However, changing γ also changed the total area under $f(x,t)$ as can be seen in the indefinite integral of $f(x,t)$:

$$\int_{-\infty}^{\infty} f(x,t)dx = \frac{2ln(e^{\gamma\tau}+1)}{\gamma} \tag{A4}$$

Thus, ranges defined by different γ values could also result in different range-wide carrying capacities, potentially altering both the ecological (e.g. through stochastic extinction events) and evolutionary (e.g. through more mutations arising in larger populations) dynamics of the ranges. Additionally, different combinations of γ and τ could result in different range widths, which have been shown to impact the dispersal distance necessary for population persistence (Van Kirk and Lewis, 1997). To control for these confounding factors, we fixed the range widths for all scenarios and altered K_{max} to maintain a constant range-wide carrying capacity. Specifically, we defined the range width using the x coordinates at which $f(x,t)$ fell below 0.1 on either side of β_t and chose τ and γ values for each scenario such that $f(x,t)$ fell below 0.1 at the same x coordinates (Table A2). We then adjusted K_{max} for each scenario so that the range-wide carrying capacity was constant (Fig. A3).

[Figure A3 goes here]

Thus, γ and τ were both fixed within a given simulation and β_t (the location of the range center) was used to simulate climate change. During the periods before and after climate change β_t was constant, but to simulate climate change it varied with time as follows

$$\beta_t = v\eta(t-\hat{t}) \tag{A5}$$

Range edge starkness	Environmental gradient	γ	τ	λ	K_{max}
Shallow	Flat	0.0025	-240	0	240
	Shallow	0.0025	-240	0.004	240
	Steep	0.0025	-240	0.008	240
Moderate	Flat	0.0075	345.9	0	118.1
	Shallow	0.0075	345.9	0.004	118.1
	Steep	0.0075	345.9	0.008	118.1
Stark	Flat	0.25	630.1	0	66.7
	Shallow	0.25	630.1	0.004	66.7
	Steep	0.25	630.1	0.008	66.7

Table A2: Descriptions and parameter values for the 9 different experimental scenarios. As defined in the text, γ affects range edge starkness, τ affects the range width, λ is the slope of the environmental gradient, and K_{max} is the maximum carrying capacity for patches in the landscape.

where v was the velocity of climate change per generation in terms of discrete patches, t was the current generation, and $\hat{t}$ was the last generation of stable climatic conditions before the onset of climate change.

Environmental gradient. The local optimum for the niche trait ($z_{opt,x}$) varied in space according to

$$z_{opt,x} = \lambda(x - \beta_t) \tag{A6}$$

with λ determining the rate of change in the optimum across the range. Individual relative fitness ($w_{i,x}$) values were then calculated according to the following equation assuming stabilizing selection

$$w_{i,x} = e^{\frac{-(z_i - z_{opt,x})^2}{2\omega^2}} \tag{A7}$$

where ω defined the strength of stabilizing selection and z_i was an individual's niche phenotype (Lande, 1976). Thus, an individual's realized fitness was higher the closer its niche phenotype (z_i) was to the environmental gradient value of the patch it occupied ($z_{opt,x}$). All loci were assumed to contribute additively to an individual's niche value with no dominance or epistasis, meaning an individual's phenotype was simply the sum of the individual's allele values. As defined above, $z_{opt,x}$ also shifted with climate change (i.e. with β_t) as would be expected if it corresponded to a phenotypic optimum along a temperature or precipitation gradient within the range (Davis and Shaw, 2001).

Population dynamics. Population growth within each patch was modeled with a stochastic implementation of the classic Ricker model (Melbourne and Hastings, 2008; Ricker, 1954). To account for fitness effects on population growth, expected population growth was scaled by the mean relative fitness of individuals within the patch ($\bar{w}_x$) so that maladaptation resulted in reduced population

growth. The expected number of new offspring in patch x at time $t+1$ was given by

$$\hat{N}_{t+1,x} = \bar{w}_x F_{t,x} \frac{R}{\psi} e^{\frac{-RN_{t,x}}{K_x}} \tag{A8}$$

where $F_{t,x}$ was the number of females in patch x at time t, R was the intrinsic growth rate for the population and remained constant in both time and space, ψ was the expected sex ratio of the population, $N_{t,x}$ was the number of individuals (males and females) in patch x at time t, and K_x was the local carrying capacity based on the environmental conditions. To incorporate demographic stochasticity, the realized number of offspring for each patch was then drawn from a Poisson distribution.

$$N_{t+1,x} \sim Poisson(\hat{N}_{t+1,x}) \tag{A9}$$

Offspring parentage was assigned by random sampling of the local male and female populations (i.e. polygynandrous mating assuming a well-mixed population within each patch). The sampling was weighted by individual fitness and occurred with replacement so highly fit individuals were likely to have multiple offspring while low fitness individuals might not have had any. Each offspring inherited one allele per locus from each parent, assuming no linkage among loci. After reproduction, all members of the previous generation died and the offspring dispersed to begin the next generation. Parameters governing population dynamics (Table A3) were chosen to yield reasonable rates of population growth based on initial exploratory simulations.

Mutation. Inherited alleles were subject to mutation such that some offspring might not inherit identical copies of certain alleles from their parents. The mutation process was defined by two parameters for each trait T: the diploid mutation rate (U^T) and the mutational variance (V_m^T). Using these parameters along with the number of loci defining trait T (L^T), the per locus probability of a mutation was

$$\frac{U^T}{2L^T} \tag{A10}$$

Parameter	Description	Value
R	Intrinsic growth rate of the population	2
ψ	Expected sex ratio (proportion of females) in the population	0.5
$\hat{d}$	Maximum achievable dispersal phenotype	1000
ρ	Determines the slope of the transition in dispersal phenotypes from 0 to D	0.5

Table A3: Values and descriptions for parameters related to population growth and dispersal.

Effect sizes of mutations were drawn from a normal distribution with mean 0 and a standard deviation of

$$\sqrt{V_m^T U^T} \tag{A11}$$

meaning the ratio of small effect to large effect mutations depended on both U^T and V_m^T. We chose parameter values (Table A4) in keeping with previously derived values from the literature (Gilbert et al., 2017). For the number of loci used in our simulations, these resulted in mostly mutations of small effect with few large effect mutations. Importantly, by defining the mutation process in this way, rather than with a per locus probability of mutation and a mutation effect size directly, the mutational input per generation was kept constant regardless of the number of loci defining the trait (Schiffers et al., 2014).

Dispersal. Finally, individuals dispersed according to an exponential dispersal kernel defined by each individual's dispersal phenotype. An individual's dispersal phenotype was the expected

Parameter	Description	Value
ω	Defines the strength of stabilizing selection on fitness traits	3
U^T	Diploid mutation rate for each trait	0.02
V_m^T	Mutational variance for each trait	0.0004
L^T	Number of diploid loci defining each trait	5 loci
μ_1^f	Initial mean allele value for the niche trait	0
μ_1^d	Initial mean allele value for the dispersal trait	-1
σ_1^f	Initial standard deviation of allele values for the niche trait	0.025
σ_1^d	Initial standard deviation of allele values for the dispersal trait	1

Table A4: Values and descriptions for parameters defining the genetic components of the model.

dispersal distance and was given by

$$d_i = \frac{\hat{d}\eta e^{\rho \Sigma L^D}}{1 + e^{\rho \Sigma L^D}} \tag{A12}$$

where $\hat{d}$ was the maximum expected dispersal distance in terms of discrete patches, ρ was a constant determining the slope of the transition between 0 and $\hat{d}$, and the summation was taken across all alleles contributing to dispersal. Thus, as with fitness, loci were assumed to contribute additively with no dominance or epistasis. The expected dispersal distance, d_i was then used to draw a realized distance from an exponential dispersal kernel. The direction of dispersal (in radians) was drawn from a uniform distribution bounded by 0 and 2π. If a dispersal trajectory took an individual outside the bounds of the landscape in the *y* dimension, the individual reappeared at the same *x* coordinate but the opposite end of the *y* dimension, thus wrapping the top and bottom edges of the landscape to avoid edge effects. Dispersal occurred from the center of each patch and the individual's new patch was then determined according to its location in the overlaid grid of η x η patches (see Figure A1). Dispersal parameters (Table A3) were chosen to allow a wide range of dispersal phenotypes to evolve in the context of the different experimental scenarios, ranging from highly restrictive to long-distance dispersal.

Appendix B: Supplementary results for varying speeds of climate change

Extinction probability

As in the main text, we calculated the cumulative probability of extinction for both slow and fast speeds of climate change. The figures in this section use the same layout and color scheme as Figure 2 in the main text to allow for direct comparisons.

[Figures B1&B2 go here.]

Dispersal evolution

Patterns in the spatial distributions of dispersal phenotypes and genetic variance largely followed similar patterns at slow and fast speeds of climate change as shown in the main text for a moderate speed of climate change. The main difference seems to be the number of populations able to track climate change when it progresses at different speeds. As in the previous section, all figures use the same layout and color scheme as Figures 3 & 4 in the main text.

[Figures B3-B6 go here.]

Adaptation to the environmental gradient

As with dispersal evolution, the spatial patterns in adaptation to the environmental gradient and genetic variance of the niche trait were broadly similar at varying speeds of climate change. One important difference, likely related to the reduced extinction risk experienced at low speeds of climate change, is that the mismatch between phenotypes and the environmental gradient imposed

by range shifting seems to be reduced at a slow speed of climate change. Thus, while fitness was still reduced in these scenarios, it was reduced less than scenarios experiencing faster speeds of climate change. Again, all figures use the same layout and color scheme as Figures 5 & 6 to allow for direct comparisons.

[Figures B7-B10 go here.]

Literature Cited

Aguilée, R., G. Raoul, F. Rousset, and O. Ronce. 2016. Pollen dispersal slows geographical range shift and accelerates ecological niche shift under climate change. Proceedings of the National Academy of Sciences 113:E5741–E5748.

Alleaume-Benharira, M., I. Pen, and O. Ronce. 2006. Geographical patterns of adaptation within a species? range: interactions between drift and gene flow. Journal of evolutionary biology 19:203–215.

Atkins, K., and J. Travis. 2010. Local adaptation and the evolution of species' ranges under climate change. Journal of Theoretical Biology 266:449–457.

Boeye, J., J. M. Travis, R. Stoks, and D. Bonte. 2013. More rapid climate change promotes evolutionary rescue through selection for increased dispersal distance. Evolutionary Applications 6:353–364.

Brooker, R. W., J. M. Travis, E. J. Clark, and C. Dytham. 2007. Modelling species' range shifts in a changing climate: the impacts of biotic interactions, dispersal distance and the rate of climate change. Journal of Theoretical Biology 245:59–65.

Case, T. J., and M. L. Taper. 2000. Interspecific competition, environmental gradients, gene flow, and the coevolution of species' borders. The American Naturalist 155:583–605.

Chen, I.-C., J. K. Hill, R. Ohlemüller, D. B. Roy, and C. D. Thomas. 2011. Rapid range shifts of species associated with high levels of climate warming. Science 333:1024–1026.

Chen, X., X. Zhang, J. A. Church, C. S. Watson, M. A. King, D. Monselesan, B. Legresy, and

573 C. Harig. 2017. The increasing rate of global mean sea-level rise during 1993–2014. Nature Climate Change 7:492.

Dallas, T., R. R. Decker, and A. Hastings. 2017. Species are not most abundant in the centre of
576 their geographic range or climatic niche. Ecology Letters 20:1526–1533.

Davis, M. B., and R. G. Shaw. 2001. Range shifts and adaptive responses to quaternary climate change. Science 292:673–679.

579 Ellner, S. 1996. Environmental fluctuations and the maintenance of genetic diversity in age or stage-structured populations. Bulletin of Mathematical Biology 58:103–127.

Excoffier, L., M. Foll, and R. J. Petit. 2009. Genetic consequences of range expansions. Annual
582 Review of Ecology, Evolution, and Systematics 40:481–501.

Fisher, R. A. 1937. The wave of advance of advantageous genes. Annals of eugenics 7:355–369.

Fronhofer, E. A., and F. Altermatt. 2015. Eco-evolutionary feedbacks during experimental range
585 expansions. Nature Communications 6:6844.

García-Ramos, G., and M. Kirkpatrick. 1997. Genetic models of adaptation and gene flow in peripheral populations. Evolution 51:21–28.

588 Gaston, K. J. 2009. Geographic range limits: achieving synthesis. Proceedings of the Royal Society B: Biological Sciences 276:1395–1406.

Gilbert, K. J., N. P. Sharp, A. L. Angert, G. L. Conte, J. A. Draghi, F. Guillaume, A. L. Harg-
591 reaves, R. Matthey-Doret, and M. C. Whitlock. 2017. Local adaptation interacts with expansion load during range expansion: Maladaptation reduces expansion load. The American Naturalist 189:368–380.

Gonzalez, P., R. P. Neilson, J. M. Lenihan, and R. J. Drapek. 2010. Global patterns in the vulnerability of ecosystems to vegetation shifts due to climate change. Global Ecology and Biogeography 19:755–768.

Grimm, V., U. Berger, D. L. DeAngelis, J. G. Polhill, J. Giske, and S. F. Railsback. 2010. The odd protocol: a review and first update. Ecological Modelling 221:2760–2768.

Hargreaves, A., S. Bailey, and R. A. Laird. 2015. Fitness declines towards range limits and local adaptation to climate affect dispersal evolution during climate-induced range shifts. Journal of Evolutionary Biology 28:1489–1501.

Hargreaves, A. L., and C. G. Eckert. 2014. Evolution of dispersal and mating systems along geographic gradients: implications for shifting ranges. Functional Ecology 28:5–21.

Hastings, A., K. Cuddington, K. F. Davies, C. J. Dugaw, S. Elmendorf, A. Freestone, S. Harrison, M. Holland, J. Lambrinos, U. Malvadkar, et al. 2005. The spatial spread of invasions: new developments in theory and evidence. Ecology Letters 8:91–101.

Henry, R. C., G. Bocedi, and J. M. Travis. 2013. Eco-evolutionary dynamics of range shifts: elastic margins and critical thresholds. Journal of Theoretical Biology 321:1–7.

Hereford, J. 2009. A quantitative survey of local adaptation and fitness trade-offs. The American Naturalist 173:579–588.

Hobbs, R. J., E. Higgs, and J. A. Harris. 2009. Novel ecosystems: implications for conservation and restoration. Trends in Ecology & Evolution 24:599–605.

Holt, R. D., T. H. Keitt, M. A. Lewis, B. A. Maurer, and M. L. Taper. 2005. Theoretical models of species? borders: single species approaches. Oikos 108:18–27.

615 Keitt, T. H., M. A. Lewis, and R. D. Holt. 2001. Allee effects, invasion pinning, and species? borders. The American Naturalist 157:203–216.

Kirkpatrick, M., and N. H. Barton. 1997. Evolution of a species' range. The American Naturalist
618 150:1–23.

Kubisch, A., T. Degen, T. Hovestadt, and H. J. Poethke. 2013. Predicting range shifts under global change: the balance between local adaptation and dispersal. Ecography 36:873–882.

621 Lande, R. 1976. Natural selection and random genetic drift in phenotypic evolution. Evolution 30:314–334.

Lenormand, T. 2002. Gene flow and the limits to natural selection. Trends in Ecology & Evolution
624 17:183–189.

Loarie, S. R., P. B. Duffy, H. Hamilton, G. P. Asner, C. B. Field, and D. D. Ackerly. 2009. The velocity of climate change. Nature 462:1052.

627 Melbourne, B. A., and A. Hastings. 2008. Extinction risk depends strongly on factors contributing to stochasticity. Nature 454:100.

Ochocki, B. M., and T. E. Miller. 2017. Rapid evolution of dispersal ability makes biological
630 invasions faster and more variable. Nature Communications 8:14315.

Parmesan, C. 2006. Ecological and evolutionary responses to recent climate change. Annual Review of Ecology, Evolution, and Systematics 37:637–669.

633 Phillips, B. L. 2015. Evolutionary processes make invasion speed difficult to predict. Biological Invasions 17:1949–1960.

Polechova, J. 2018. Is the sky the limit? on the expansion threshold of a species? range. PLoS biology 16:e2005372.

Polechová, J., and N. H. Barton. 2015. Limits to adaptation along environmental gradients. Proceedings of the National Academy of Sciences page 201421515.

Price, T. D., and M. Kirkpatrick. 2009. Evolutionarily stable range limits set by interspecific competition. Proceedings of the Royal Society B: Biological Sciences 276:1429–1434.

Ricker, W. E. 1954. Stock and recruitment. Journal of the Fisheries Board of Canada 11:559–623.

Schiffers, K., F. M. Schurr, J. M. Travis, A. Duputié, V. M. Eckhart, S. Lavergne, G. McInerny, K. A. Moore, P. B. Pearman, W. Thuiller, et al. 2014. Landscape structure and genetic architecture jointly impact rates of niche evolution. Ecography 37:1218–1229.

Schwartz, M. W., L. R. Iverson, A. M. Prasad, S. N. Matthews, and R. J. O'Connor. 2006. Predicting extinctions as a result of climate change. Ecology 87:1611–1615.

Sexton, J. P., P. J. McIntyre, A. L. Angert, and K. J. Rice. 2009. Evolution and ecology of species range limits. Annu. Rev. Ecol. Evol. Syst. 40:415–436.

Shaw, A. K., C. C. D?Aloia, and P. M. Buston. 2019. The evolution of marine larval dispersal kernels in spatially structured habitats: Analytical models, individual-based simulations, and comparisons with empirical estimates. The American Naturalist 193:000–000.

Shaw, A. K., M. Jalasvuori, and H. Kokko. 2014. Population-level consequences of risky dispersal. Oikos 123:1003–1013.

Shaw, A. K., and H. Kokko. 2015. Dispersal evolution in the presence of allee effects can speed up or slow down invasions. The American Naturalist 185:631–639.

Shine, R., G. P. Brown, and B. L. Phillips. 2011. An evolutionary process that assembles phenotypes through space rather than through time. Proceedings of the National Academy of Sciences 108:5708–5711.

Szűcs, M., M. Vahsen, B. Melbourne, C. Hoover, C. Weiss-Lehman, and R. Hufbauer. 2017. Rapid adaptive evolution in novel environments acts as an architect of population range expansion. Proceedings of the National Academy of Sciences 114:13501–13506.

Team, R. C. 2000. R language definition. Vienna, Austria: R Foundation for Statistical Computing .

Thuiller, W., S. Lavorel, and M. B. Araújo. 2005. Niche properties and geographical extent as predictors of species sensitivity to climate change. Global Ecology and Biogeography 14:347–357.

Van Kirk, R. W., and M. A. Lewis. 1997. Integrodifference models for persistence in fragmented habitats. Bulletin of Mathematical Biology 59:107.

Wallace, B. 1975. Hard and soft selection revisited. Evolution 29:465–473.

Weiss-Lehman, C., R. A. Hufbauer, and B. A. Melbourne. 2017. Rapid trait evolution drives increased speed and variance in experimental range expansions. Nature Communications 8:14303.

672

Figures

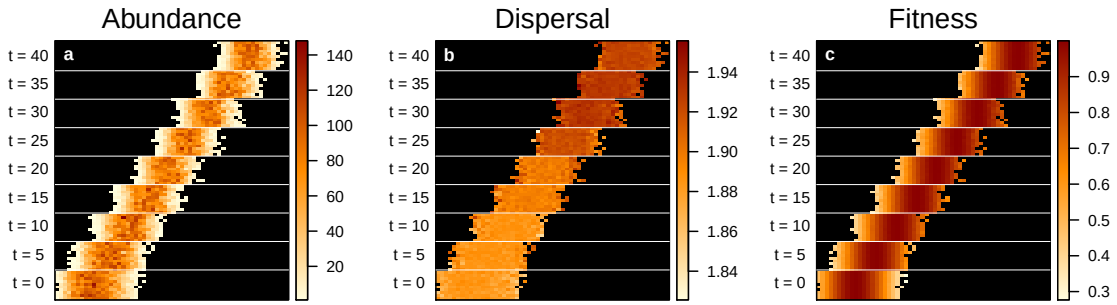

Figure 1: A single example of a simulation with a steep environmental gradient and a moderately stark range edge. Information on the (a) abundance, (b) dispersal ability, and (c) fitness of individuals in each patch is shown for time periods beginning with the last generation of stable climate conditions ($t = 0$) to 40 generations after the start of climate change. Log transformed mean dispersal phenotypes (b) are shown for each patch. Average patch fitness (c) was calculated based on the mean niche trait of local individuals and the gradient value at each patch.

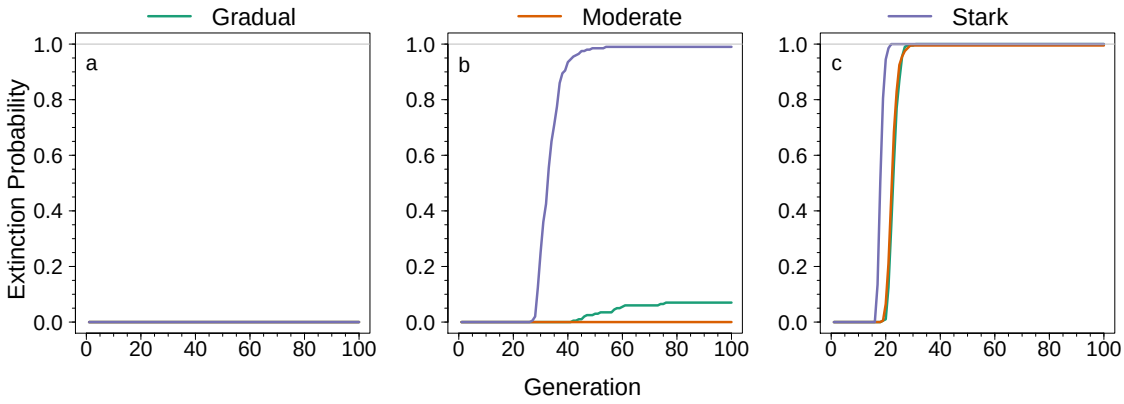

Figure 2: The cumulative probability of extinction due to a moderate speed of climate change in different experimental scenarios. Graphs show the proportion of simulated populations that went extinct through time for scenarios with a (a) flat, (b) shallow, and (c) steep environmental gradient, and in ranges characterized by shallow, moderate, or stark edges, indicated by line color as shown in the legend. In all graphs, a horizontal grey line shows 100% extinction.

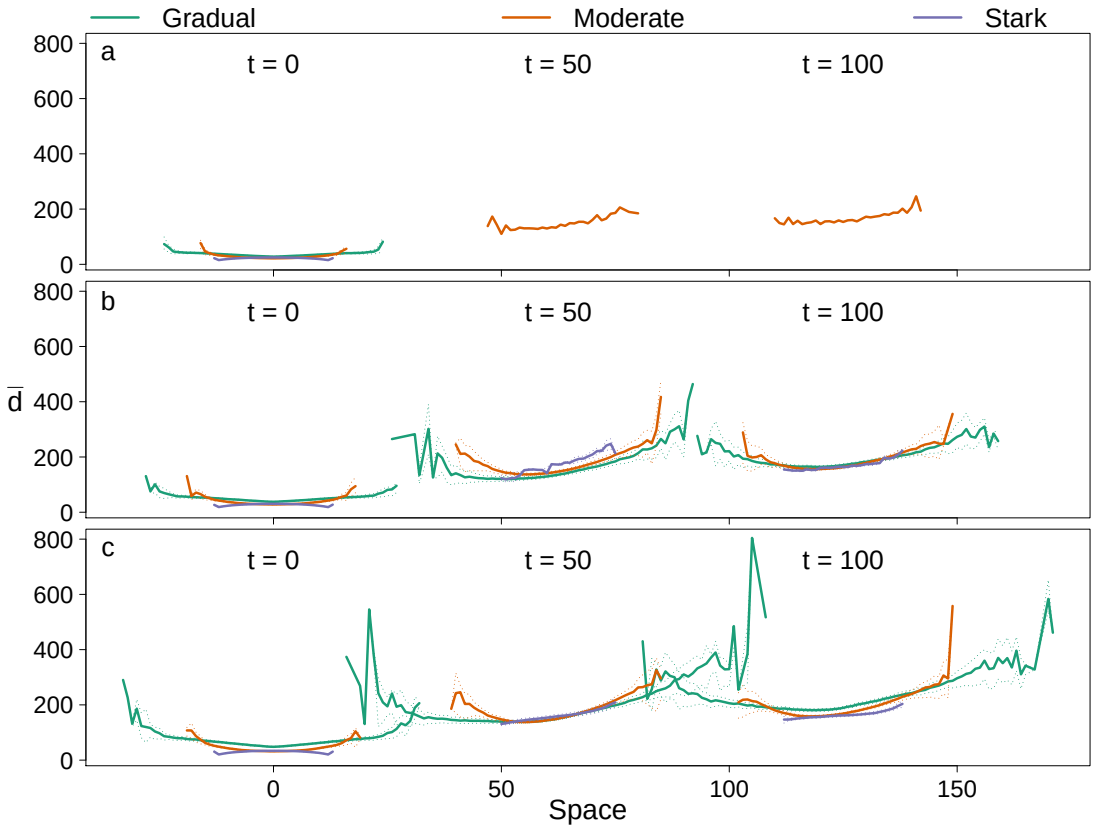

Figure 3: Spatial distributions of dispersal phenotypes at three different time points during climate change. Solid lines indicate the average dispersal phenotype at each x coordinate and dotted lines are the interquartile ranges of patch means. Means and interquartile ranges were calculated across the pooled patch level means along the y dimension of each simulation at each x coordinate. Graphs show the spatial distributions of dispersal phenotypes in scenarios with (a) steep, (b) shallow, and (c) flat environmental gradients. Colors indicate different edge types as shown in the figure legend. Results are shown for the equilibrium distribution ($t = 0$), halfway through climate change ($t = 50$), and the end of climate change ($t = 100$) and a moderate speed of climate change.

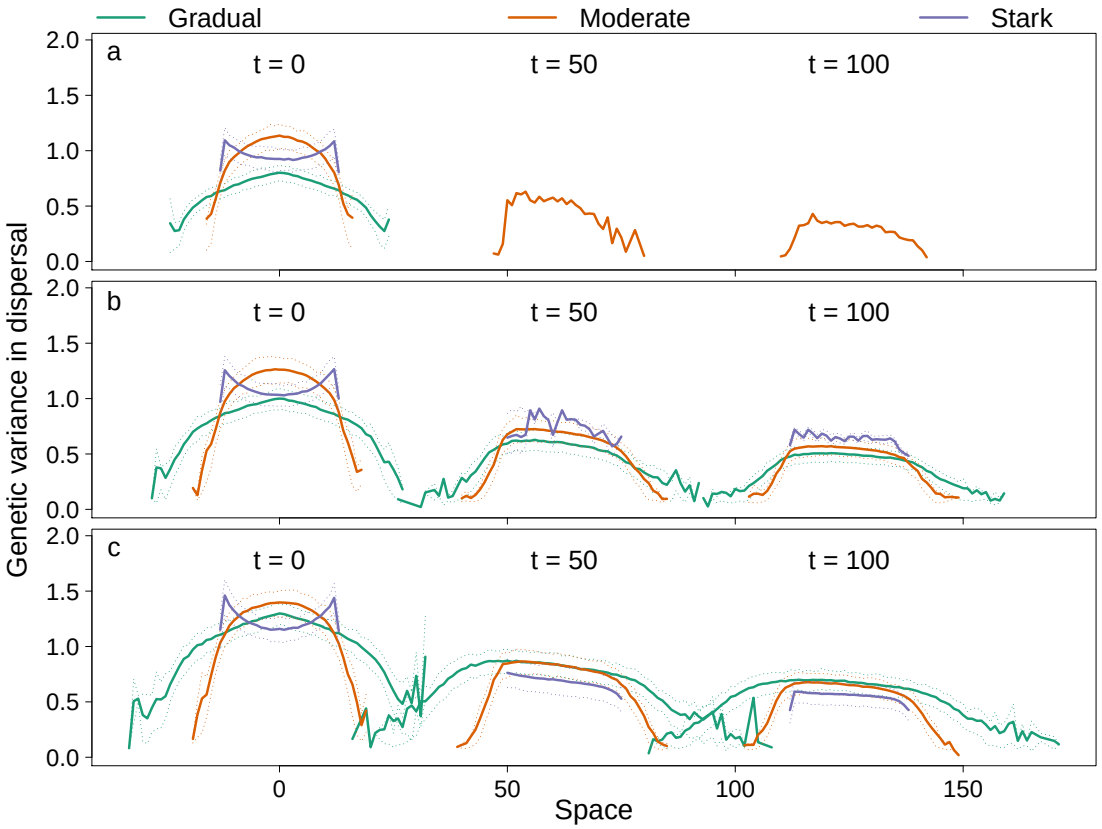

Figure 4: Spatial distributions of genetic variance in dispersal at three different time points during climate change. Solid lines indicate the average genetic variance of patches at each x coordinate and dotted lines are the interquartile ranges. Means and interquartile ranges were calculated across the pooled patch level variances along the y dimension of each simulation at each x coordinate. Graphs show the spatial distributions of genetic variance in dispersal in scenarios with (a) steep, (b) shallow, and (c) flat environmental gradients. Colors indicate different edge types as shown in the figure legend. Results are shown for the equilibrium distribution ($t = 0$), halfway through climate change ($t = 50$), and the end of climate change ($t = 100$) and a moderate speed of climate change.

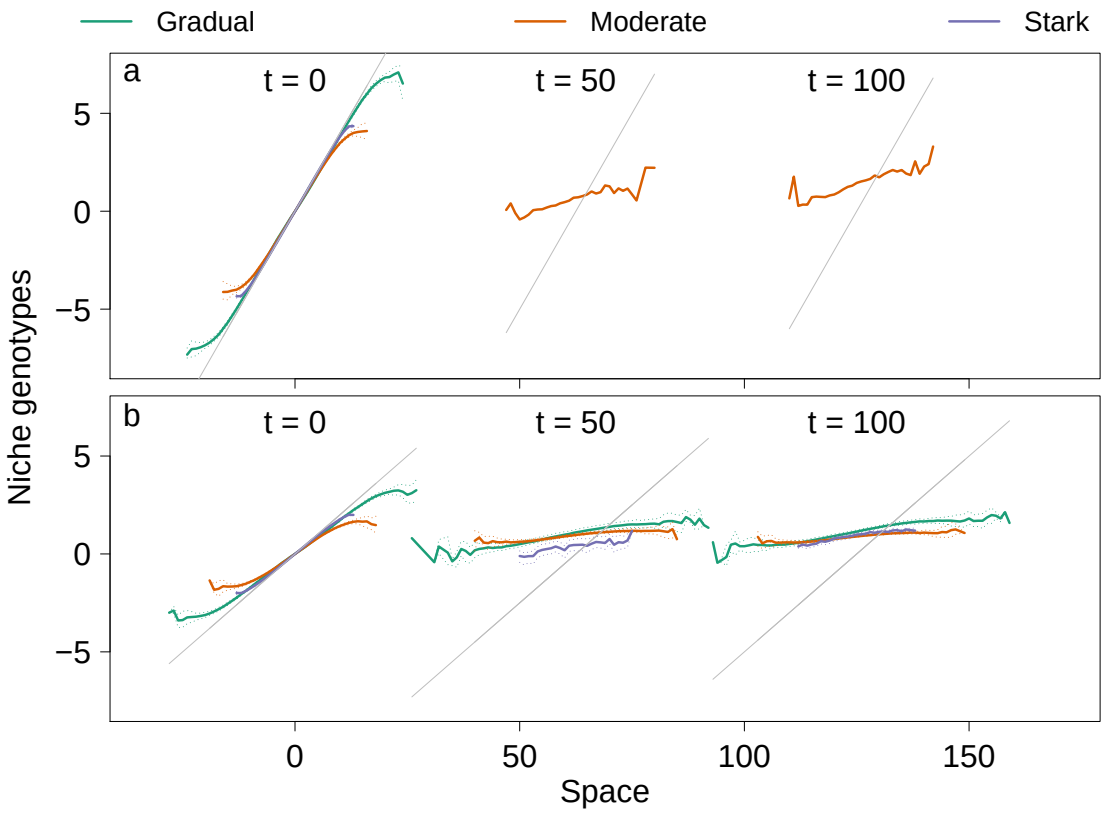

Figure 5: Spatial distributions of niche trait phenotypes at three different time points during climate change. Solid lines indicate the average phenotype at each x coordinate and dotted lines are the interquartile ranges of patch means. Means and interquartile ranges were calculated across the pooled patch level means along the y dimension of each simulation at each x coordinate. Graphs show the spatial distributions of niche trait phenotypes in scenarios with (a) steep, (b) shallow, and (c) flat environmental gradients. Colors indicate different edge types as shown in the figure legend. Results are shown for the equilibrium distribution ($t = 0$), halfway through climate change ($t = 50$), and the end of climate change ($t = 100$) and a moderate speed of climate change.

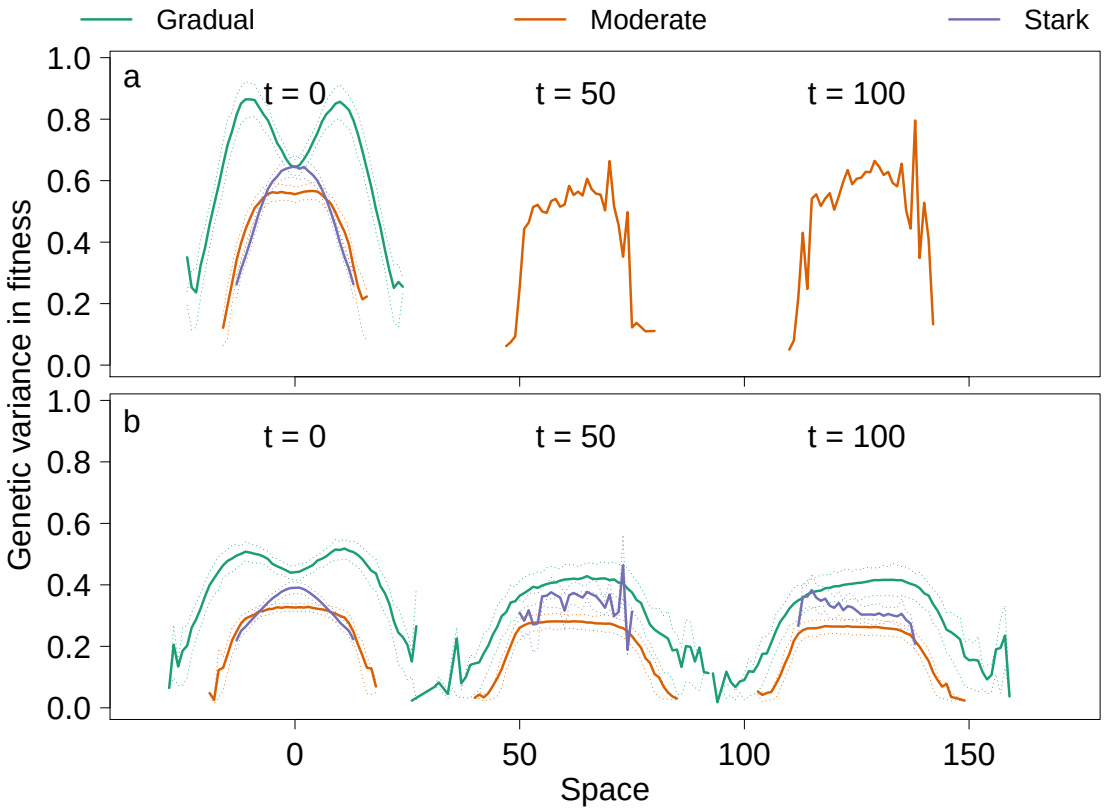

Figure 6: Spatial distributions of genetic variance in the niche trait at three different time points during climate change. Solid lines indicate the average genetic variance of patches at each x coordinate and dotted lines are the interquartile ranges. Means and interquartile ranges were calculated across the pooled patch level variances along the y dimension of each simulation at each x coordinate. Graphs show the spatial distributions of genetic variance in the niche trait in scenarios with (a) steep, (b) shallow, and (c) flat environmental gradients. Colors indicate different edge types as shown in the figure legend. Results are shown for the equilibrium distribution ($t = 0$), halfway through climate change ($t = 50$), and the end of climate change ($t = 100$) and a moderate speed of climate change.

Online figures

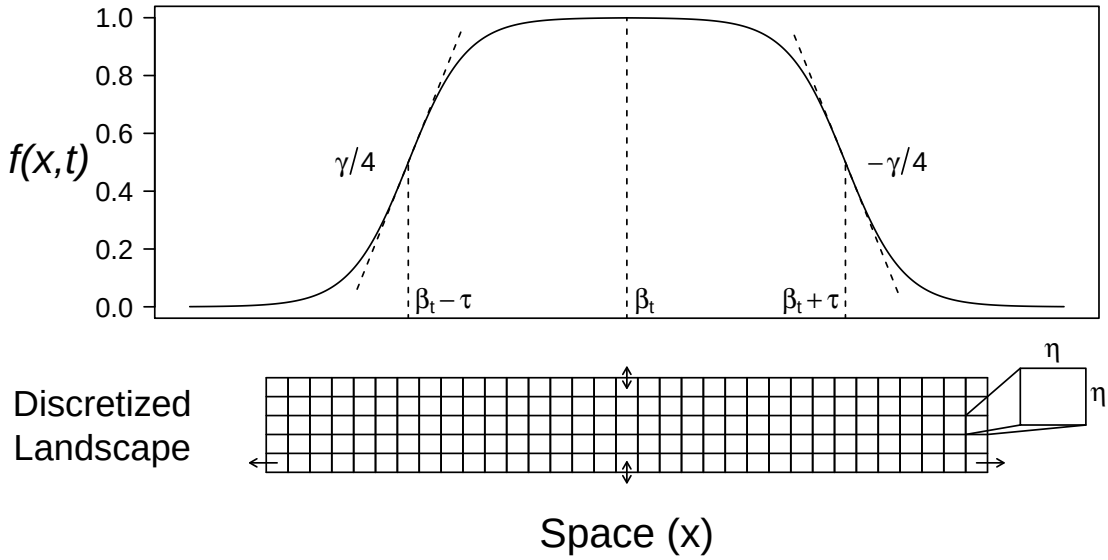

Figure A1: Example visualization of $f(x,t)$ in Cartesian space. The parameters of $f(x,t)$ are shown on the figure at significant points along the x axis. Specifically, β_t defined the range center, γ determined the slope of $f(x,t)$ at the inflection points (i.e. the range edges), and τ determined the location of the inflection points. The lattice of discrete η x η patches in which population dynamics occurred is shown beneath. As described in the *Submodels* section of Appendix A, $f(x,t)$ determined the carrying capacity of the patches along the x dimension of the lattice while carrying capacity remained constant within each column along the y dimension. Landscapes were unbounded in the x dimension and implemented with wrapping boundaries in the y dimension.

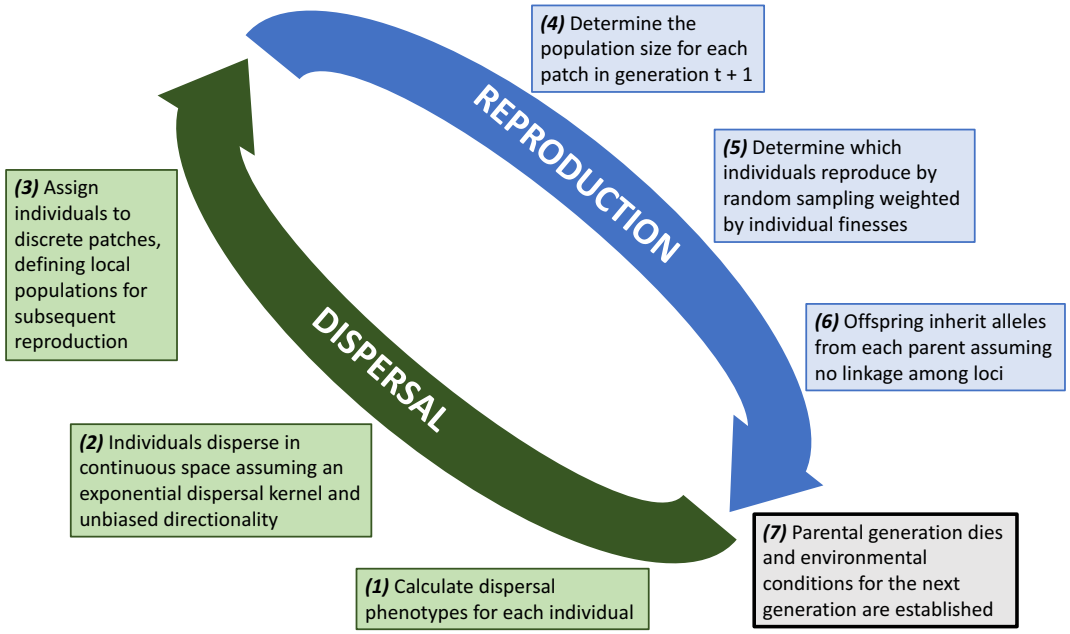

Figure A2: The life cycle of simulated populations is shown divided between events contributing to reproduction and dispersal. Each generation began with new offspring dispersing according to their phenotype, after which reproduction occurred in local populations defined by the discrete lattice. After reproduction, all parental individuals perished, resulting in discrete, non-overlapping generations.

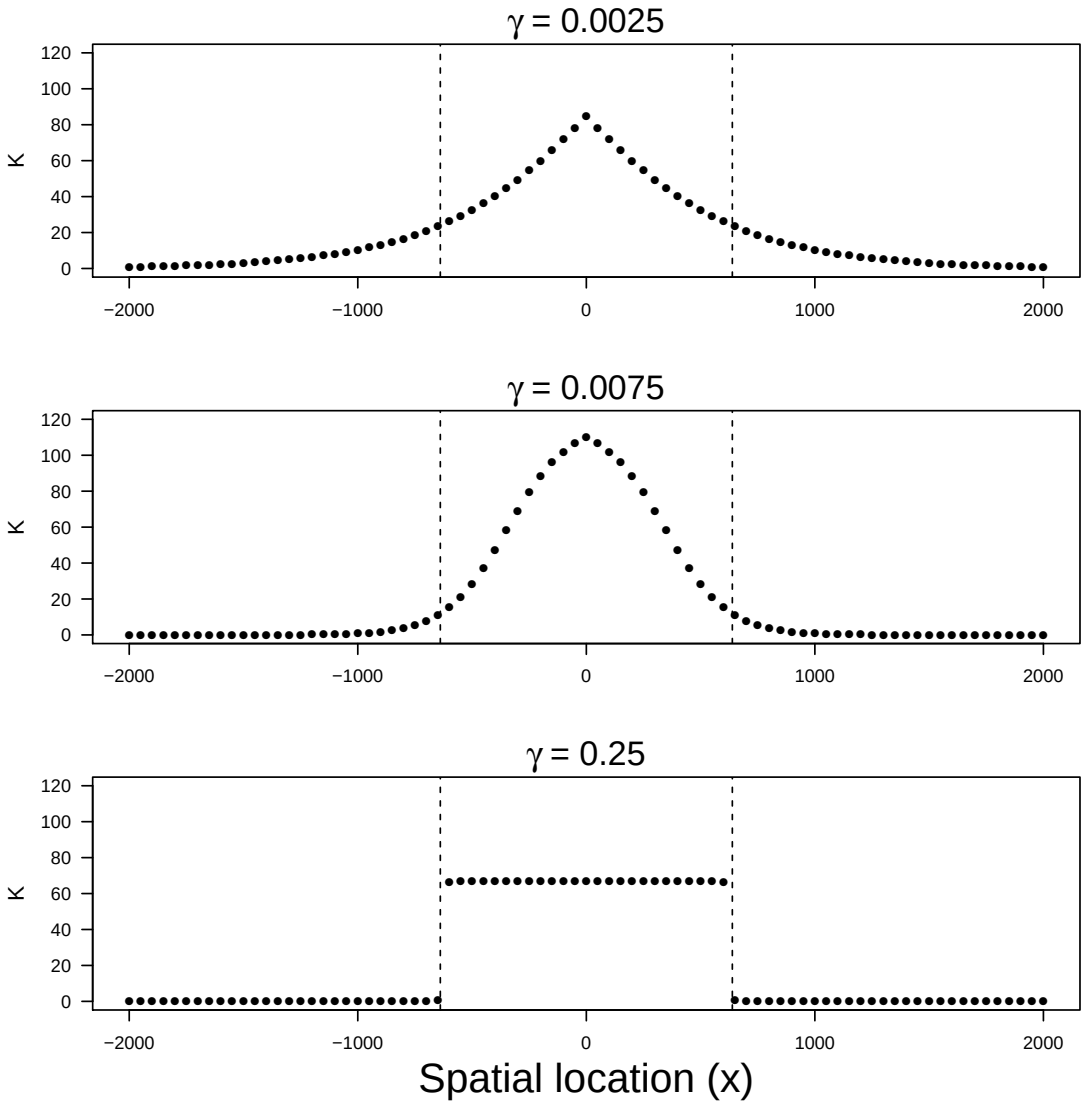

Figure A3: The carrying capacity of discrete patches along the x dimension of landscapes. From top to bottom, the plots show the carrying capacities for gradual, moderate, and stark range edges. Points represent the carrying capacity of a discrete η x η patch in the range. The vertical dashed lines indicate the x coordinates at which $f(x,t)$ declines below 0.1 and the γ value for each plot is listed above. Parameter values correspond to those listed in Table A2.

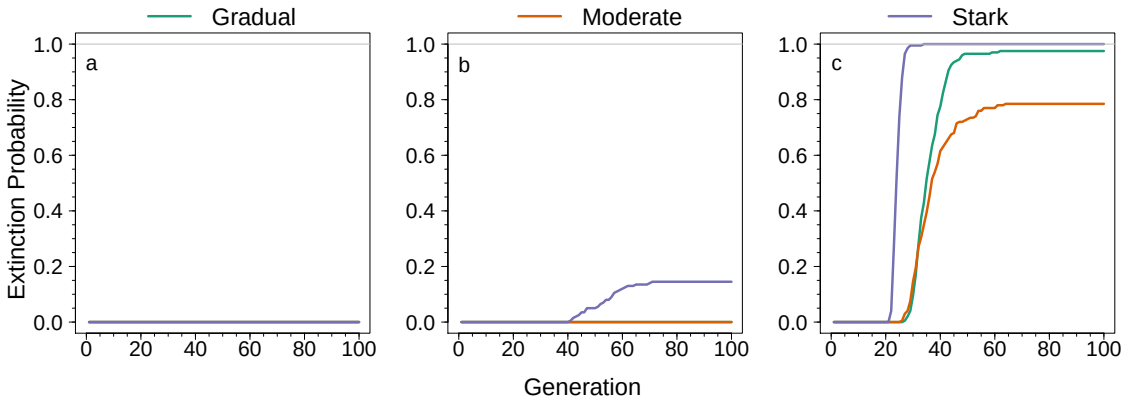

Figure B1: The cumulative probability of extinction due to a slow speed of climate change in different experimental scenarios. Graphs show the proportion of simulated populations that went extinct through time for scenarios with a (a) flat, (b) shallow, and (c) steep environmental gradient, and in ranges characterized by shallow, moderate, or stark edges, indicated by line color as shown in the legend. In all graphs, a horizontal grey line shows 100% extinction.

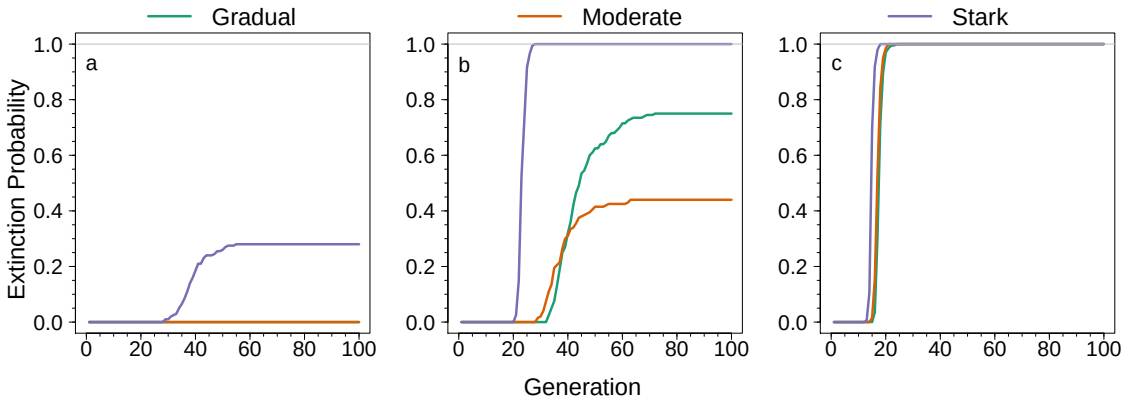

Figure B2: The cumulative probability of extinction due to a fast speed of climate change in different experimental scenarios. Graphs show the proportion of simulated populations that went extinct through time for scenarios with a (a) flat, (b) shallow, and (c) steep environmental gradient, and in ranges characterized by shallow, moderate, or stark edges, indicated by line color as shown in the legend. In all graphs, a horizontal grey line shows 100% extinction.

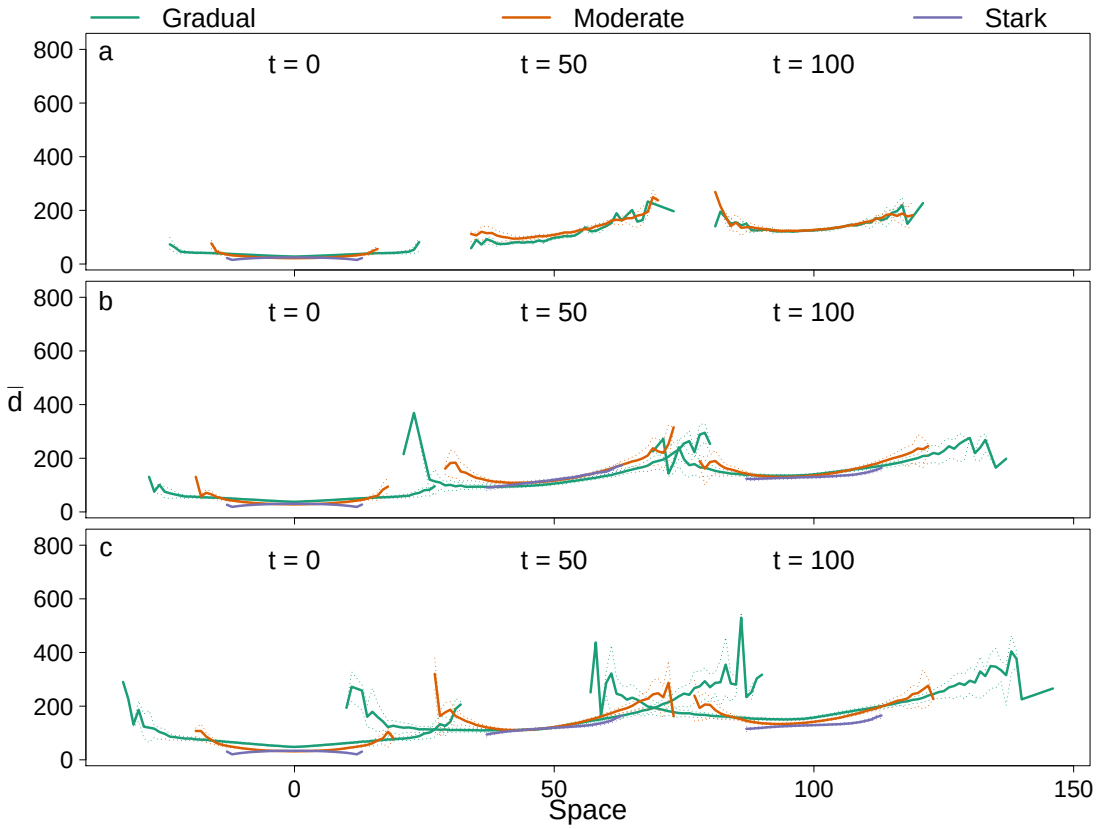

Figure B3: Spatial distributions of dispersal phenotypes at three different time points during climate change. Solid lines indicate the average dispersal phenotype at each x coordinate and dotted lines are the interquartile ranges of patch means. Means and interquartile ranges were calculated across the pooled patch level means along the y dimension of each simulation at each x coordinate. Graphs show the spatial distributions of dispersal phenotypes in scenarios with (a) steep, (b) shallow, and (c) flat environmental gradients. Colors indicate different edge types as shown in the figure legend. Results are shown for the equilibrium distribution ($t = 0$), halfway through climate change ($t = 50$), and the end of climate change ($t = 100$) and a slow speed of climate change.

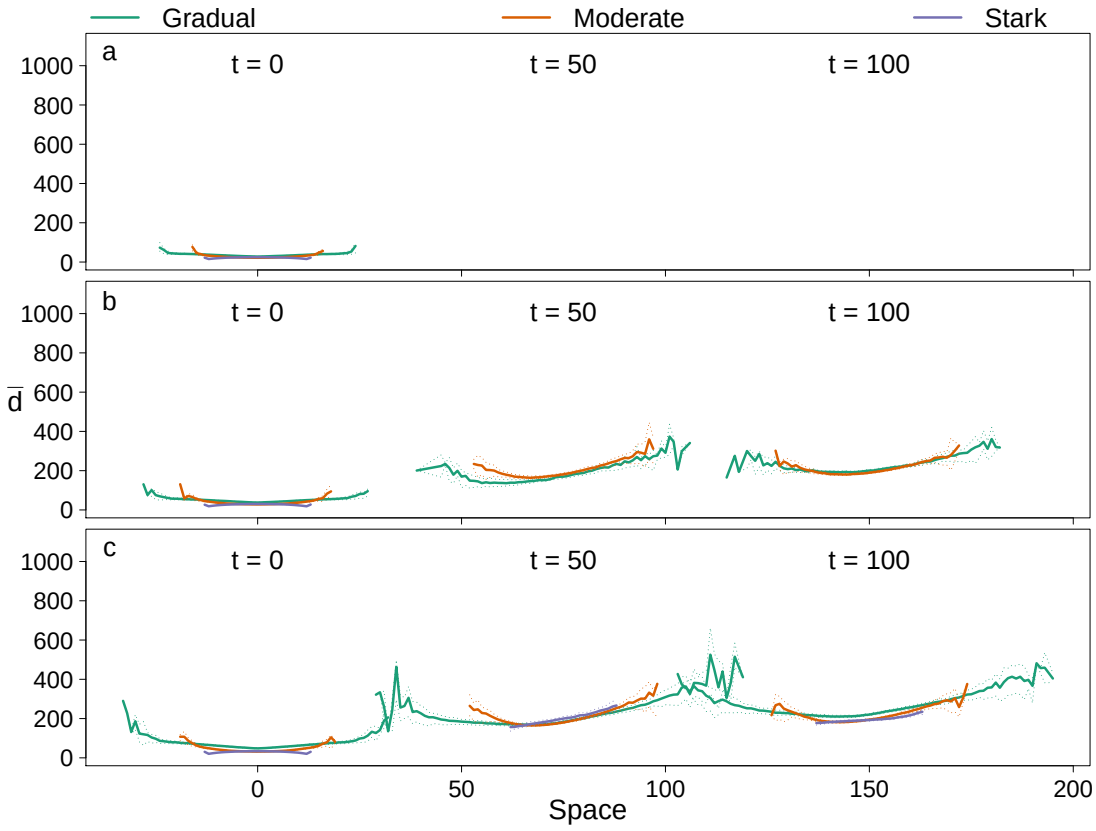

Figure B4: Spatial distributions of dispersal phenotypes at three different time points during climate change. Solid lines indicate the average dispersal phenotype at each x coordinate and dotted lines are the interquartile ranges of patch means. Means and interquartile ranges were calculated across the pooled patch level means along the y dimension of each simulation at each x coordinate. Graphs show the spatial distributions of dispersal phenotypes in scenarios with (a) steep, (b) shallow, and (c) flat environmental gradients. Colors indicate different edge types as shown in the figure legend. Results are shown for the equilibrium distribution ($t = 0$), halfway through climate change ($t = 50$), and the end of climate change ($t = 100$) and a fast speed of climate change.

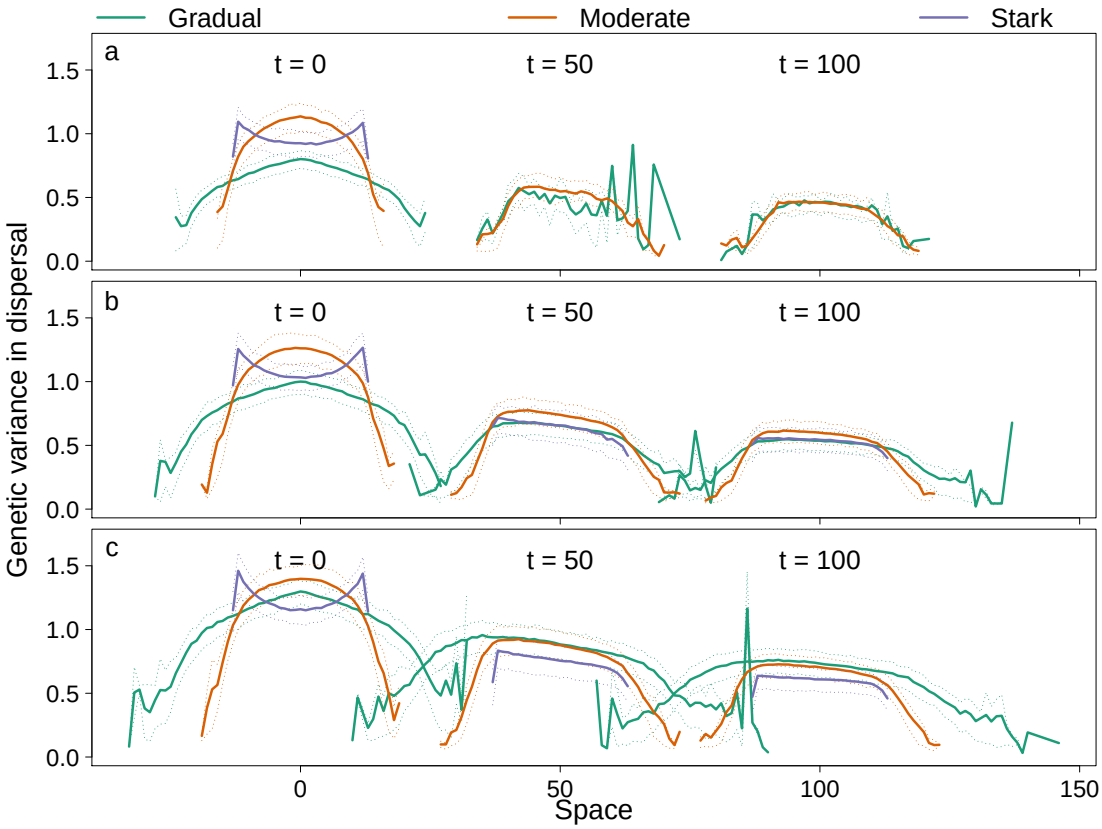

Figure B5: Spatial distributions of genetic variance in dispersal at three different time points during climate change. Solid lines indicate the average genetic variance of patches at each x coordinate and dotted lines are the interquartile ranges. Means and interquartile ranges were calculated across the pooled patch level variances along the y dimension of each simulation at each x coordinate. Graphs show the spatial distributions of genetic variance in dispersal in scenarios with (a) steep, (b) shallow, and (c) flat environmental gradients. Colors indicate different edge types as shown in the figure legend. Results are shown for the equilibrium distribution ($t = 0$), halfway through climate change ($t = 50$), and the end of climate change ($t = 100$) and a slow speed of climate change.

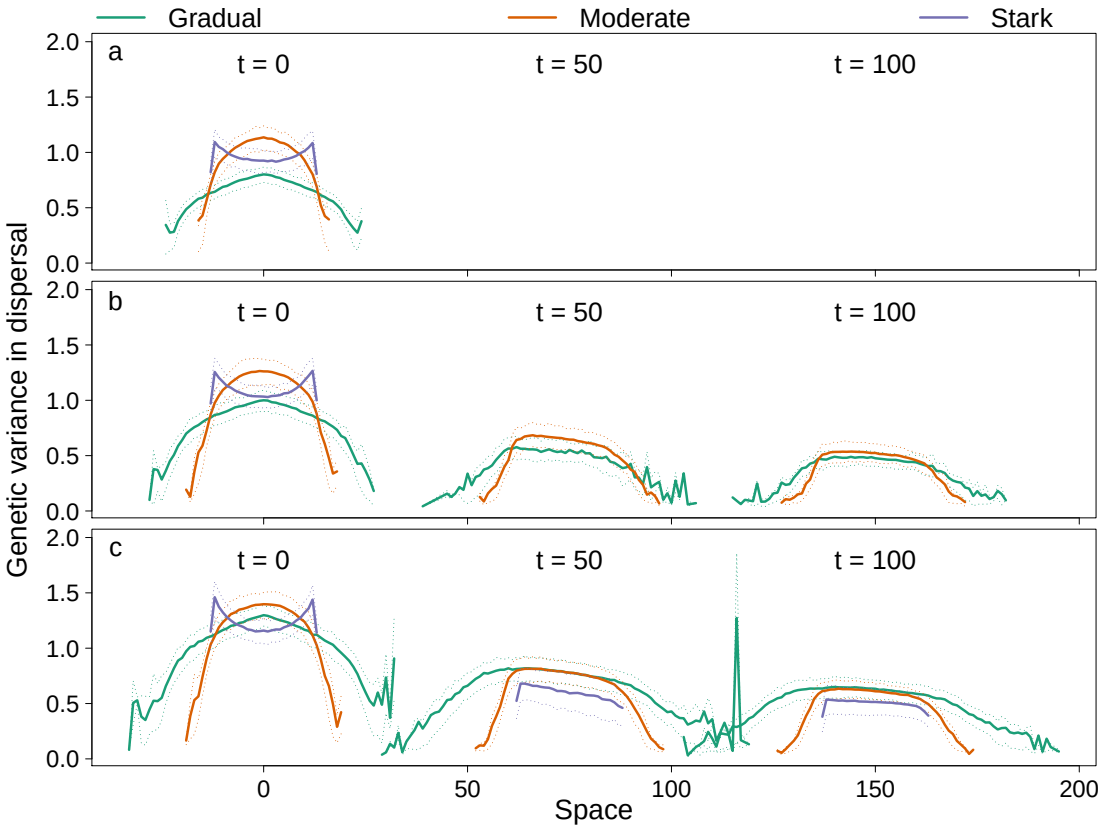

Figure B6: Spatial distributions of genetic variance in dispersal at three different time points during climate change. Solid lines indicate the average genetic variance of patches at each x coordinate and dotted lines are the interquartile ranges. Means and interquartile ranges were calculated across the pooled patch level variances along the y dimension of each simulation at each x coordinate. Graphs show the spatial distributions of genetic variance in dispersal in scenarios with (a) steep, (b) shallow, and (c) flat environmental gradients. Colors indicate different edge types as shown in the figure legend. Results are shown for the equilibrium distribution ($t = 0$), halfway through climate change ($t = 50$), and the end of climate change ($t = 100$) and a fast speed of climate change.

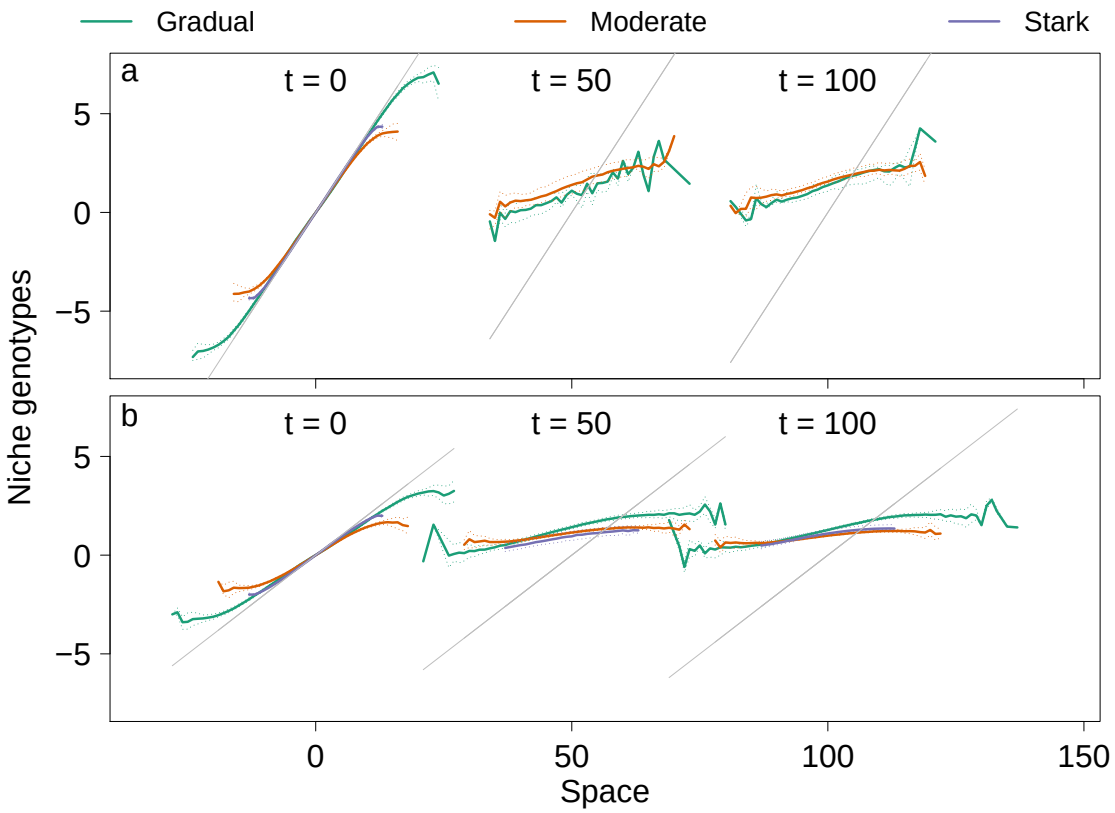

Figure B7: Spatial distributions of niche trait phenotypes at three different time points during climate change. Solid lines indicate the average phenotype at each x coordinate and dotted lines are the interquartile ranges of patch means. Means and interquartile ranges were calculated across the pooled patch level means along the y dimension of each simulation at each x coordinate. Graphs show the spatial distributions of niche trait phenotypes in scenarios with (a) steep, (b) shallow, and (c) flat environmental gradients. Colors indicate different edge types as shown in the figure legend. Results are shown for the equilibrium distribution ($t = 0$), halfway through climate change ($t = 50$), and the end of climate change ($t = 100$) and a slow speed of climate change.

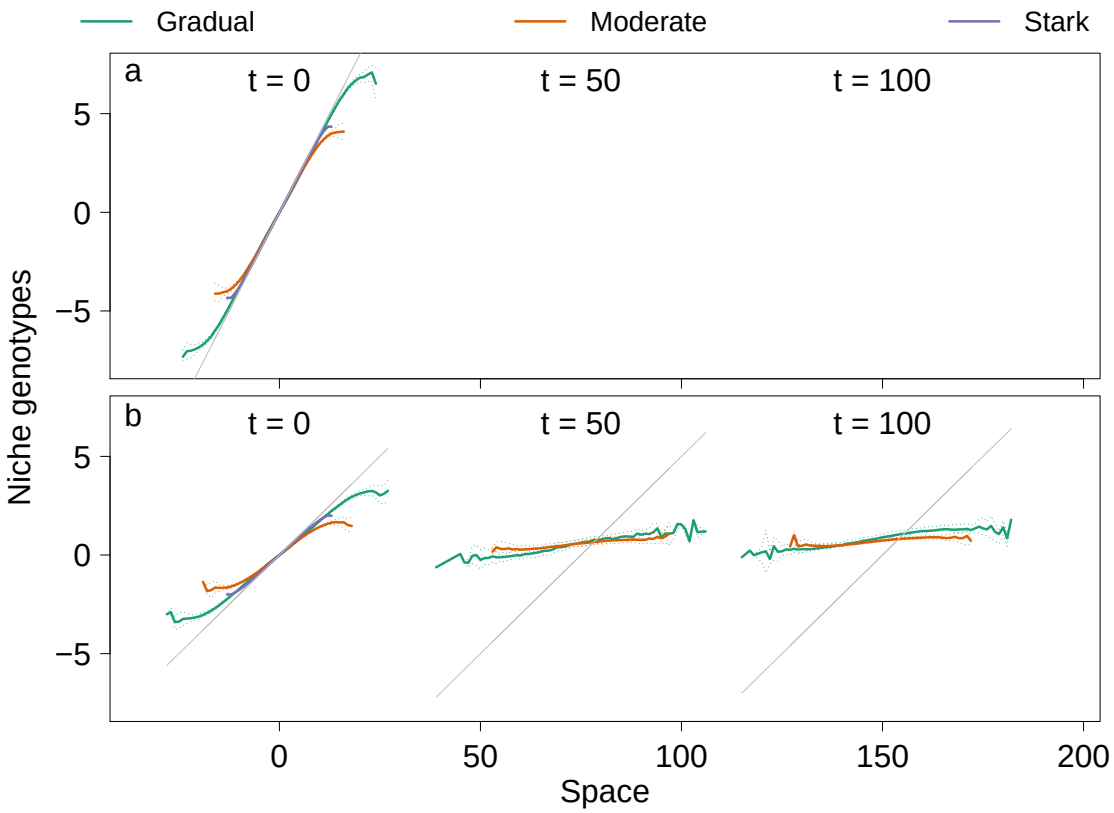

Figure B8: Spatial distributions of niche trait phenotypes at three different time points during climate change. Solid lines indicate the average phenotype at each x coordinate and dotted lines are the interquartile ranges of patch means. Means and interquartile ranges were calculated across the pooled patch level means along the y dimension of each simulation at each x coordinate. Graphs show the spatial distributions of niche trait phenotypes in scenarios with (a) steep, (b) shallow, and (c) flat environmental gradients. Colors indicate different edge types as shown in the figure legend. Results are shown for the equilibrium distribution ($t = 0$), halfway through climate change ($t = 50$), and the end of climate change ($t = 100$) and a fast speed of climate change.

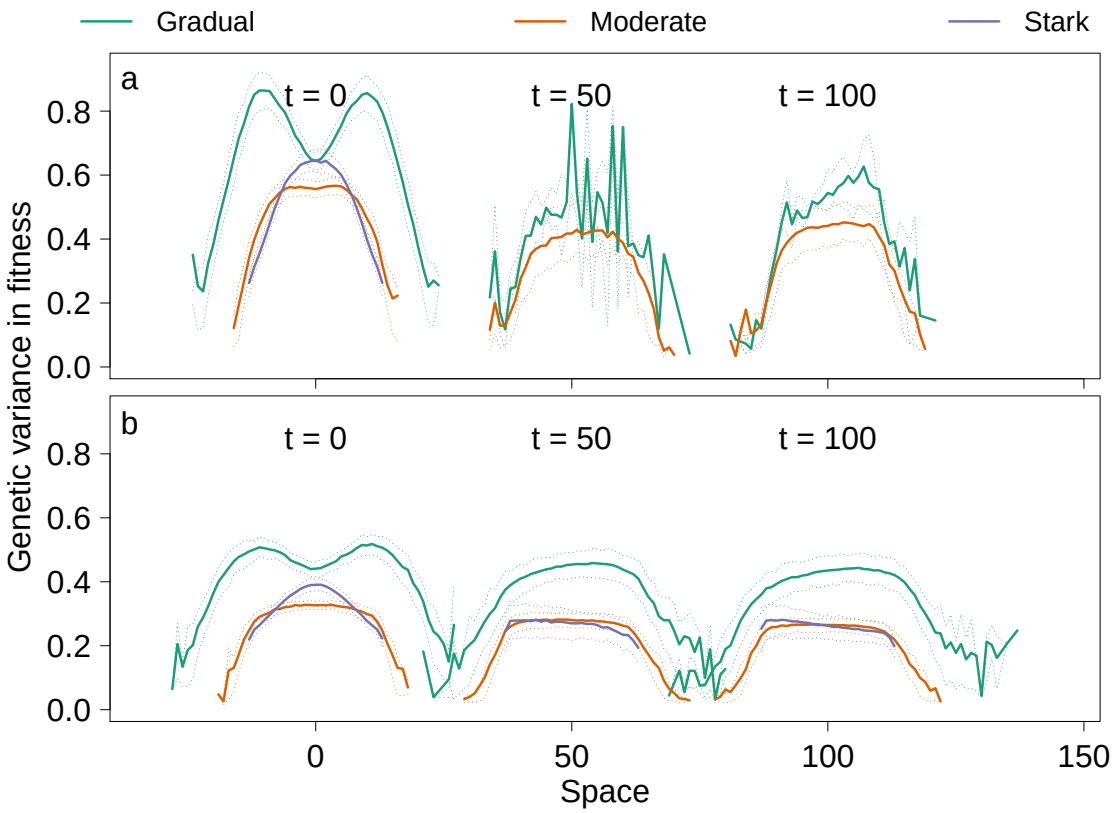

Figure B9: Spatial distributions of genetic variance in the niche trait at three different time points during climate change. Solid lines indicate the average genetic variance of patches at each x coordinate and dotted lines are the interquartile ranges. Means and interquartile ranges were calculated across the pooled patch level variances along the y dimension of each simulation at each x coordinate. Graphs show the spatial distributions of genetic variance in the niche trait in scenarios with (a) steep, (b) shallow, and (c) flat environmental gradients. Colors indicate different edge types as shown in the figure legend. Results are shown for the equilibrium distribution ($t = 0$), halfway through climate change ($t = 50$), and the end of climate change ($t = 100$) and a slow speed of climate change.

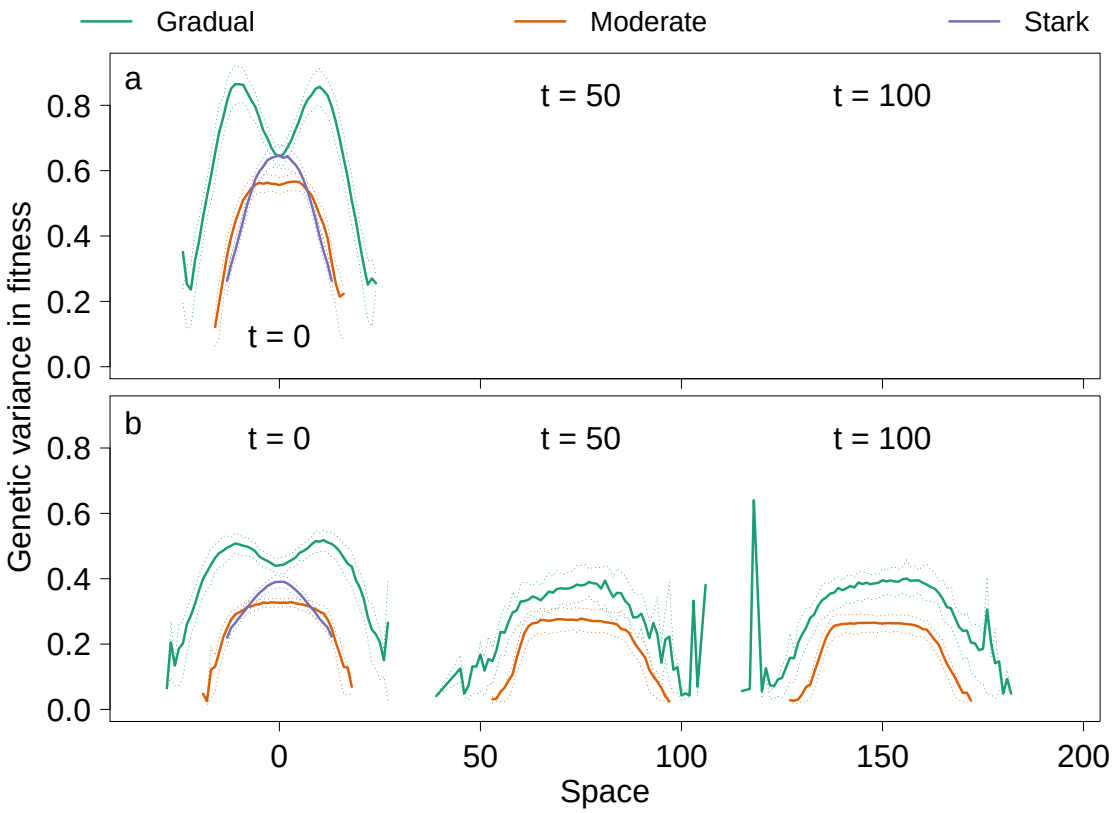

Figure B10: Spatial distributions of genetic variance in the niche trait at three different time points during climate change. Solid lines indicate the average genetic variance of patches at each x coordinate and dotted lines are the interquartile ranges. Means and interquartile ranges were calculated across the pooled patch level variances along the y dimension of each simulation at each x coordinate. Graphs show the spatial distributions of genetic variance in the niche trait in scenarios with (a) steep, (b) shallow, and (c) flat environmental gradients. Colors indicate different edge types as shown in the figure legend. Results are shown for the equilibrium distribution ($t = 0$), halfway through climate change ($t = 50$), and the end of climate change ($t = 100$) and a fast speed of climate change.